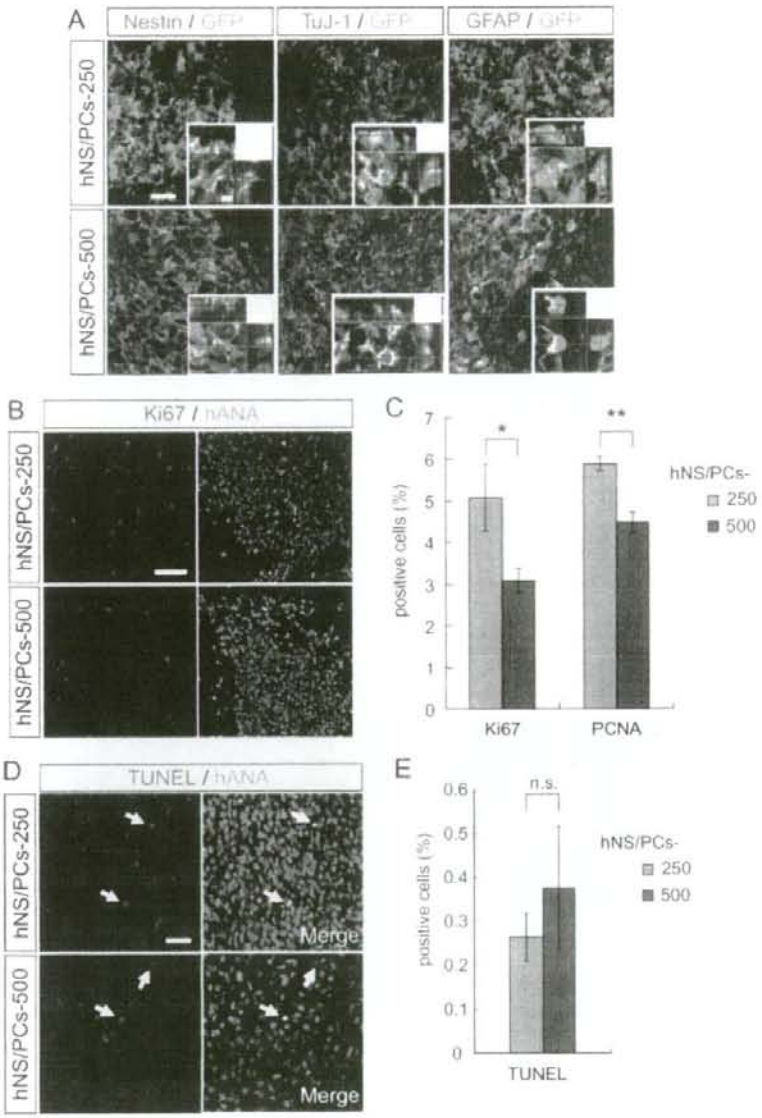

Fig. 4. Both hNS/PCs-250 and -500 appropriately differentiated into neurons and astrocytes in vivo. A: Immunofluorescence analysis of tissue sections 4 weeks after transplantation. Although some of the grafted hNS/PCs-250 and -500 still expressed Nestin, they had also differentiated into TuJ-1-positive neurons and GFAP-positive astrocytes. B: Representative image of Ki67-positive proliferating cells in the hNS/PCs-250 and -500 grafts. C: Quantitative analysis of the proportion of Ki67- and PCNA-positive cells in grafted hNS/PCs-250 and -500 4 weeks after transplantation. hNS/PCs-250 showed a significantly higher proportion of proliferating cells than did hNS/PCs-500. D: Analysis of apoptotic cells by TUNEL staining in grafted hNS/PCs. E: Quantitative analysis of TUNEL-positive cells. No significant difference in the TUNEL-positive apoptotic cells was observed between hNS/PCs-250 and -500. All data are presented as the mean 6 SEM; n 5 3. *P < 0.05; **P < 0.01; n.s., not significant. Scale bars 5 20 1m and 5 1m for low- and high-magnification images, respectively, in A; 50 1m in B; 20 1m in D.

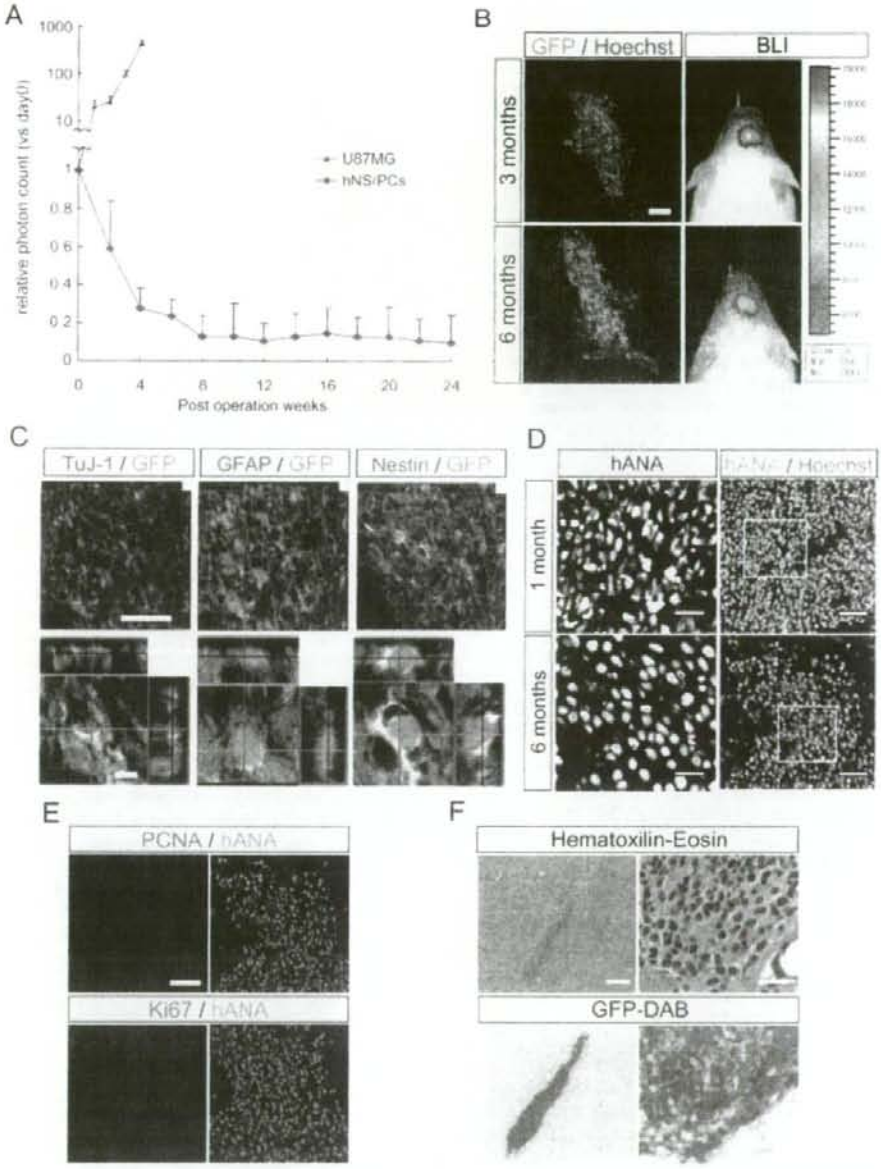

Fig. 5. hNS/PCs did not exhibit tumorigenesis for 6 months. A: Long-term observation of grafted hNS/PCs-250 by BLI for 6 months. The photon count of hNS/PCs decreased for 8 weeks after transplantation but was stable thereafter. The hNS/PCs did not show any evidence of tumorigenicity during the 6-month observation period, unlike the control U87MG cells. Data are presented as the mean 6 SEM. B: Immunohistochemical analysis of Venus-expressing grafted hNS/PCs 3 and 6 months after transplantation showed consistent correlation of the Venus-expressing area with the photon counts detected by BLI. C: Immunohistochemical analysis of grafted hNS/PCs 6 months after transplantation. hNS/PCs resided at the site of injection and differentiated into TuJ-1-positive neurons and GFAP-positive astrocytes. However, Nestin-positive neural progenitors were also observed, even 6 months after transplantation. D: hANA and Hoechst nuclear staining of the grafted area 1 month and 6 months after the transplantation. Grafted cells showed larger nuclei and lower cell densities in the long-term analysis than in the short-term analysis. E: Immunohistochemical analysis of proliferation markers PCNA and Ki67. Neither PCNA- nor Ki67-positive cells were observed. F: Hematoxylin-eosin and GFP-DAB staining indicated no malignant invasive features in the transplanted cells. Scale bars 5 100 1m in B; low-magnification image 50 1m, high-magnification image 5 1m in C; low-magnification image 50 1m, high-magnification image 20 1m in D; 50 1m in E; low-magnification image 200 1m, high-magnification image 20 1m in F.

these findings indicate that the grafted hNS/PCs could survive and differentiate properly in the brain of NOD/SCID mice without any tumor formation, at least for 6 months after transplantation.

DISCUSSION

Human Fetal Neurospheres Exhibited Altered Proliferation and Differentiation Properties In Vitro and In Vivo, Depending on the Culture Period

Because large numbers of human fetus-derived cells are difficult to obtain unless they are expanded in vitro, it is essential to evaluate the differentiation and proliferation properties as well as tumorigenic potential of in-vitro-expanded hNS/PCs when considering their clinical use in cell replacement therapies. In the present study, we clearly showed the likely senescence of hNS/PCs maintained for more than 500 DIV, from their differentiation and proliferation properties. More importantly, we also showed the lack of tumorigenicity of hNS/PCs-250 over the long term in vivo. This is the first report in which the in vivo tumorigenicity of transplanted in-vitro-maintained hNS/PCs was evaluated by long-term monitoring with BLI.

The in vitro ATP assay (Fig. 1A) and in vivo BLI study (Fig. 3A) showed that hNS/PCs-250 had significantly higher growth and survival rates than did hNS/PCs-500 both in vitro and in vivo. This difference between hNS/PCs-250 and -500 in vitro was attributable to a reduced proportion of dividing cells in the hNS/PCs-500, shown by positive staining for Ki67 or PCNA, or in the cell cycle of S/G2/M, but not to the proportion of annexin V-positive apoptotic cells. In addition, the proportion of $CD133^+$ undifferentiated hNS/PCs was lower in the older hNS/PCs-500 than in the younger hNS/PCs-250. Thus, hNS/PCs seem to lose their ability to self-renew and acquire the properties of committed progenitors or postmitotic cells during their long-term culture in vitro.

Interestingly, this difference in self-renewability between hNS/PCs-250 and -500 seemed to be correlated with an alteration in their differentiation potentials. hNS/PCs-250 exhibited more neurogenic and fewer gliogenic properties than hNS/PCs-500 (Fig. 2A,B). Given that the $CD24^+$ cells are proposed to be associated with the population of committed neuronal progenitors and neurons (Calaora et al., 1996; Shewan et al., 1996; Doetsch et al., 1999; Murayama et al., 2002; Nieoullon et al., 2005; Pruszak et al., 2007), the significantly higher proportion of $CD24^+$ cells in hNS/PCs-250 than in hNS/PCs-500 (Fig. 2C,D) also supports the idea that the hNS/PCs-250 contain more neurogenic progenitors than do the hNS/PCs-500, which contain more gliogenic progenitors. Taken together, these findings suggest that human fetal neurospheres lose multipotent and self-renewable hNS/PCs, which are replaced by progenitors committed to become glial cells, after long-term maintenance in vitro.

Long-Term Observation by BLI Revealed hNS/PCs To Be Nontumorigenic up to 6 Months After Their Transplantation Into NOD/SCID Striatum

Although some reports have examined the safety of grafted cells, including their long-term potential for tumorigenicity, by histological analyses, this type of analysis does not allow the dynamics of donor cells to be observed over time in the same live animal. In the present study, we monitored the survival of hNS/PCs grafted into the NOD/SCID striatum by BLI. Because we do not have to sacrifice the animals at each time point for histological analysis, we can repeatedly examine the same grafted animal and sequentially evaluate the in vivo tumorigenicity of the donor cells. This monitoring system allows a more accurate analysis than the conventional intermittent histological method.

The findings that the photon counts of engrafted hNS/PCs-250 decreased to 12.8% of the initial count within 8 weeks after transplantation and that their signals were maintained thereafter for up to 6 months without any tumorigenic proliferation, unlike the U87MG glioblastoma cell line, suggested that hNS/PCs-250 are not tumorigenic. These results were confirmed by histological analyses. The Venus-positive area 6 months after transplantation was no greater than the area 3 months after the surgery. No Ki67- or PCNA-positive proliferative cells were observed 6 months after the transplantation. HE staining indicated a pathology that lacked any malignant invasive behavior. Taken together, these results strongly indicate that the hNS/PCs-250 were negative for tumorigenicity. Surprisingly, the Venus-positive grafted cells were still positive for Nestin even 6 months after the transplantation, but they were negative for the proliferation markers Ki67 and PCNA (Fig. 5E). Moreover, the density of the grafted cells was much lower in animals 6 months after grafting than 1 month after grafting (Fig. 5D). Although we cannot clarify the properties of these Nestin-positive but proliferation marker-negative cells, they might reside in the grafted sites as dormant neural stem cells. Therefore, further evaluation of the safety of these donor cells, such as observation periods much longer than 6 months, is warranted.

In conclusion, we showed that the maintenance and safety of transplanted hNS/PCs could be assessed by monitoring the dynamics of these cells in vivo using BLI. Our present study provides a reliable system for evaluating the tumorigenicity of hNS/PCs in vivo and addresses several issues that are prerequisites for the clinical application of hNS/PCs, including defining their properties in vitro and in vivo and their tumorigenicity when transplanted after long-term maintenance in culture. Taken together with previous reports, our data indicate that the prospect for the future application of hNS/PCs to cell replacement therapies for neurological disorders is very promising.

ACKNOWLEDGMENTS

We are grateful to Dr. S. Mitani for the anti-GFP antibody; Drs. T. Nomura and K. Tamaoki for the NOG mice; Dr. M. Yamasaki for the human neural

stem/progenitor cells; Dr. H. Miyoshi for the lenti-virus vector; Dr. Y. Toyama for continuous encouragement; Mrs. Y. Yamashita, Ms. A. Yokokawa, and Mrs. T. Harada for technical assistance; and all the members of Dr. Okano's laboratory for encouragement and kind support.

REFERENCES

Anderson L, Burnstein RM, He X, Luce R, Furlong R, Foltynie T, Sykacek P, Menon DK, Caldwell MA. 2007. Gene expression changes in long term expanded human neural progenitor cells passaged by chopping lead to loss of neurogenic potential in vivo. Exp Neurol 204:512–524.

Barraud P, Stott S, Mollgard K, Parmar M, Anders B. 2007. In vitro characterization of a human neural progenitor cell coexpressing SSEA4 and CD133. J Neurosci Res 85:250–259.

Calaora V, Chazal G, Nielsen PJ, Rougon G, Moreau H. 1996. mCD24 expression in the developing mouse brain and in zones of secondary neurogenesis in the adult. Neuroscience 73:581–594.

Caldwell MA, He X, Wilkie N, Pollack S, Marshall G, Wafford KA, Svendsen CN. 2001. Growth factors regulate the survival and fate of cells derived from human neurospheres. Nat Biotechnol 19:475–479.

Carpenter MK, Cui X, Hu Z, Jackson J, Sherman S, Seiger A, Wahlberg LU. 1999. In vitro expansion of a multipotent population of human neural progenitor cells. Exp Neurol 158:265–278.

Crouch SPM, Kozlowski R, Slater KJ, Fletcher J. 1993. The use of ATP bioluminescence as a measure of cell proliferation and cytotoxicity. J Immunol Methods 160:81–88.

Cummings BJ, Uchida N, Tamaki SJ, Salazar DL, Hooshmand M, Summers R, Gage FH, Anderson AJ. 2005. Human neural stem cells differentiate and promote locomotor recovery in spinal cord-injured mice. Proc Natl Acad Sci U S A 102:14069–14074.

Deitch A, Law H, deVere White R. 1982. A stable propidium iodide staining procedure for flow cytometry. J Histochem Cytochem 30:967–972.

Doetsch F, Caille I, Lim DA, Garcia-Verdugo JM, Alvarez-Buylla A. 1999. Subventricular zone astrocytes are neural stem cells in the adult mammalian brain. Cell 97:703–716.

Ito M, Hiramatsu H, Kobayashi K, Suzue K, Kawahata M, Hioki K, Ueyama Y, Koyanagi Y, Sugamura K, Tsuji K, Heike T, Nakahata T. 2002. NOD/SCID/gamma cnull mouse: an excellent recipient mouse model for engraftment of human cells. Blood 100:3175–3182.

Iwanami A, Kaneko S, Nakamura M, Kanemura Y, Mori H, Kobayashi S, Yamasaki M, Momoshima S, Ishii H, Ando K, Tanioka Y, Tamaoki N, Nomura T, Toyama Y, Okano H. 2005. Transplantation of human neural stem cells for spinal cord injury in primates. J Neurosci Res 80:182–190.

Jeong S, Chu K, Jung K, Kim SU, Kim M, Roh J-K. 2003. Human neural stem cell transplantation promotes functional recovery in rats with experimental intracerebral hemorrhage. Stroke 34:2258–2263.

Kanemura Y, Mori H, Kobayashi S, Islam O, Kodama E, Yamamoto A, Nakanishi Y, Arita N, Yamasaki M, Okano H, Hara M, Miyake J. 2002. Evaluation of in vitro proliferative activity of human fetal neural stem/progenitor cells using indirect measurements of viable cells based on cellular metabolic activity. J Neurosci Res 69:869–879.

Keyoung HM, Roy NS, Benraiss A, Louissaint A, Suzuki A, Hashimoto M, Rashbaum WK, Okano H, Goldman SA. 2001. High-yield selection and extraction of two promoter-defined phenotypes of neural stem cells from the fetal human brain. Nat Biotechnol 19:843–850.

Masuda H, Maruyama T, Hiratsu E, Yamane J, Iwanami A, Nagashima T, Ono M, Miyoshi H, Okano HJ, Ito M, Tamaoki N, Nomura T, Okano H, Matsuzaki Y, Yoshimura Y. 2007. Noninvasive and real-time assessment of reconstructed functional human endometrium in NOD/SCID/g-formula immunodeficient mice. Proc Natl Acad Sci U S A 104:1925–1930.

McBride JL, Behrstock SP, Chen E, Jakel RJ, Irwin Siegel CNS, Kordower JH. 2004. Human neural stem cell transplants improve motor function in a rat model of Huntington's disease. J Comp Neurol 475:211–219.

Miyoshi H, Blomer U, Takahashi M, Gage FH. 1998. Development of a self-inactivating lentivirus vector. J Virol 72:8150–8157.

Murayama A, Matsuzaki Y, Kawaguchi A, Shimazaki T, Okano H. 2002. Flow cytometric analysis of neural stem cells in the developing and adult mouse brain. J Neurosci Res 69:837–847.

Nakamura Y, Yamamoto M, Oda E, Yamamoto A, Kanemura Y, Hara M, Suzuki A, Yamasaki M, Okano H. 2003. Expression of tubulin beta II in neural stem/progenitor cells and radial fibers during human fetal brain development. Lab Invest 83:479–489.

Nieoullon V, Belvindrah R, Rougon G, Chazal G. 2005. mCD24 regulates proliferation of neuronal committed precursors in the subventricular zone. Mol Cell Neurosci 28:462–474.

Okada S, Ishii K, Yamane J, Iwanami A, Ikegami T, Katoh H, Iwamoto Y, Nakamura M, Miyoshi H, Okano HJ, Contag CH, Toyama Y, Okano H. 2005. In vivo imaging of engrafted neural stem cells: its application in evaluating the optimal timing of transplantation for spinal cord injury. FASEB J 19:1839–1841.

Okano H. 2002. Stem cell biology of the central nervous system. J Neurosci Res 69:698–707.

Panchision DM, Chen H-L, Pistollato F, Papini D, Ni H-T, Hawley TS. 2007. Optimized flow cytometric analysis of central nervous system tissue reveals novel functional relationships among cells expressing CD133, CD15, and CD24. Stem Cells 25:1560–1570.

Petty RD, Sutherland LA, Hunter EM, Cree IA. 1995. Comparison of MTT and ATP-based assays for the measurement of viable cell number. J Biolumin Chemilumin 10:29–34.

Piao J, Odeberg J, Samuelsson EB, Kjaeldgaard A, Falci S, Seiger A, Sundstrom E, Akesson E. 2006. Cellular composition of long-term human spinal cord- and forebrain-derived neurosphere cultures. J Neurosci Res 84:471–482.

Pruszak J, Sonntag KC, Aung MH, Sanchez-Pernaute R, Isacson O. 2007. Markers and methods for cell sorting of human embryonic stem cell-derived neural cell populations. Stem Cells 25:2257–2268.

Reynolds B, Weiss S. 1992. Generation of neurons and astrocytes from isolated cells of the adult mammalian central nervous system. Science 255:1707–1710.

Shewan D, Calaora V, Nielsen P, Cohen J, Rougon G, Moreau H. 1996. mCD24, a glycoprotein transiently expressed by neurons, is an inhibitor of neurite outgrowth. J Neurosci 16:2624–2634.

Shultz L, Schweitzer P, Christianson S, Gott B, Schweitzer I, Tennent B, McKenna S, Mobraaten L, Rajan T, Greiner D. 1995. Multiple defects in innate and adaptive immunologic function in NOD/LtSz-scid mice. J Immunol 154:180–191.

Svendsen CN, ter Borg MG, Armstrong RJE, Rosser AE, Chandran S, Ostenfeld T, Caldwell MA. 1998. A new method for the rapid and long term growth of human neural precursor cells. J Neurosci Methods 85:141–152.

Uchida N, Buck DW, He D, Reitsma MJ, Masek M, Phan TV, Tsukamoto AS, Gage FH, Weissman IL. 2000. Direct isolation of human central nervous system stem cells. Proc Natl Acad Sci U S A 97:14720–14725.

Vescovi AL, Parati EA, Gritti A, Poulin P, Ferrario M, Wanke E, Frolichsthal-Schoeller P, Cova L, Arcellana-Panlilio M, Colombo A, Galli R. 1999. Isolation and cloning of multipotential stem cells from the embryonic human CNS and establishment of transplantable human neural stem cell lines by epigenetic stimulation. Exp Neurol 156:71–83.

Wright LS, Prowse KR, Wallace K, Linskens MHK, Svendsen CN. 2006. Human progenitor cells isolated from the developing cortex undergo decreased neurogenesis and eventual senescence following expansion in vitro. Exp Cell Res 312:2107–2120.

Interferon-α 2b–induced thrombocytopenia is caused by inhibition of platelet production but not proliferation and endomitosis in human megakaryocytes

*Akiko Yamane,[1] *Takanori Nakamura,[1,2] Hidenori Suzuki,[3] Mamoru Ito,[4] Yasuyuki Ohnishi,[4] Yasuo Ikeda,[1] and Yoshitaka Miyakawa[1]

[1]Division of Hematology, Department of Internal Medicine, Keio University School of Medicine, Tokyo; [2]Biological Research Laboratories, Nissan Chemical Industries, Saitama; [3]Medical Research and Development Center, Tokyo Metropolitan Institute of Medical Science, Tokyo; and [4]Central Institute for Experimental Animals, Kanagawa, Japan

Human interferon (IFN)- is the standard therapy for chronic hepatitis C to prevent its progression to liver cirrhosis and hepatocellular carcinoma. Thrombocytopenia is one of the major adverse effects of IFN- and often leads to dose reduction or treatment discontinuation. However, there is little information on how IFN- inhibits human megakaryopoiesis. In this study, we demonstrated that IFN- did not inhibit colony formation of megakaryocytes from human CD34 hematopoietic stem cells. IFN- did not inhibit endomitosis but did inhibit cytoplasmic maturation of megakaryocytes and platelet production in vitro. IFN- suppressed the expression of transcription factors regulating late-stage megakaryopoiesis, such as GATA-1, p45^{NF-E2}, and MafG. IFN- also significantly reduced the number of human platelets but not megakaryocytes, and did not inhibit endomitosis of human megakaryocytes in immunodeficient NOD/Shi-*scid*/IL-2R ^{null} (NOG) mice transplanted with human CD34 cells (hu-NOG). We also demonstrated that a novel thrombopoietin mimetic, NIP-004, was effective for treating IFN- –induced thrombocytopenia in hu-NOG mice. From ultrastructural study, IFN- inhibited the maturation of demarcation membranes in megakaryocytes, although NIP-004 prevented the inhibitory effects of IFN- . These results defined the pathogenesis of IFN- –induced thrombocytopenia and suggested possible future clinical applications for thrombopoietin mimetics. (Blood. 2008;112: 542-550)

Introduction

Human interferon (IFN)- is the standard treatment for patients with chronic hepatitis C.[1,2] It is well known that chronic hepatitis C can lead to liver cirrhosis and hepatocellular carcinoma; the risk of progression to cirrhosis within 5 years is approximately 40%.[3] Among patients with compensated liver cirrhosis, the probability of its transition to decompensated cirrhosis and hepatocellular carcinoma within 5 years is approximately 20% and 10%, respectively.[4,5] Thus, it is important for chronic hepatitis C patients to receive IFN- treatment to prevent malignant transformation by eradicating hepatitis C virus.[6-11] However, IFN- –induced thrombocytopenia often leads to dose reduction or discontinuation of IFN- therapy. In particular, it is difficult to treat patients with advanced cirrhosis by IFN- because often these patients also have severe thrombocytopenia.

Several studies have suggested that IFN- induces thrombocytopenia by inhibiting the proliferation of human megakaryocytes, as the number of colony-forming units of megakaryocytes (CFU-MK) is reduced by relatively high concentrations of IFN- in vitro.[12-15] In clinical studies, however, the administration of human IFN- to patients with chronic hepatitis, solid tumors, and myeloproliferative disorders does not affect the number of megakaryocytes in bone marrow.[16-19] We speculate that this discrepancy is caused by differences in the dose of IFN- and hematopoietic microenvironment between CFU-MK in vitro assays and in vivo studies. Clinical studies have also proposed autoimmune reaction and capillary sequestration as causes of IFN- –induced thrombocytopenia.[18,20-22] Megakaryocytes differentiate from hematopoietic stem cells and undergo endomitosis followed by cytoplasmic maturation.[23,24] In endomitosis, megakaryocytes repeat DNA replication without cytokinesis to develop polyploidy. At the stage of cytoplasmic maturation in megakaryocytes, both the demarcation membrane system and granules develop, which enlarges the cell body. At the final stage of megakaryopoiesis, mature megakaryocytes extend thin protrusions called proplatelets, and their tips are released into the circulation as platelets. The lack of a suitable experimental animal model of human megakaryopoiesis has hampered the study of the mechanism of IFN- –induced thrombocytopenia. We recently developed a new experimental animal model of human megakaryopoiesis using immunodeficient nonobese diabetic (NOD)/Shi-*scid*/IL-2R ^{null} (NOG) mice transplanted with human CD34 cells (hu-NOG mice).[25] This prompted us to undertake this study, which investigates the mechanism of human IFN- –induced thrombocytopenia.

Thrombopoietin (TPO) is a lineage-specific cytokine that regulates both proliferation and differentiation of megakaryocytes.[26] The receptor for TPO is c-Mpl and *c-mpl*–deficient mice demonstrated severe thrombocytopenia, with an 85% reduction in the number of platelets and megakaryocytes.[27] Although several clinical trials of TPO have demonstrated that recombinant human (rh) TPO and pegylated recombinant human megakaryocyte growth and development factor (PEG-rhMGDF)

Submitted November 30, 2007; accepted April 6, 2008. Prepublished online as *Blood* First Edition paper, June 3, 2008; DOI 10.1182/blood-2007-12-125906.

*A.Y. and T.N. contributed equally to this study and should be regarded as co-first authors.

The publication costs of this article were defrayed in part by page charge payment. Therefore, and solely to indicate this fact, this article is hereby marked "advertisement" in accordance with 18 USC section 1734.

are effective for treating thrombocytopenia associated with nonmyeloablative chemotherapy, some individuals treated with PEG-rhMGDF have demonstrated thrombocytopenia because of the development of neutralizing antibodies to endogenous TPO,[28,29] which led to a clinical trial of rhTPO and PEG-rhMGDF being aborted.

Recently, second-generation of thrombopoietic growth factors such as TPO peptide (AMG 531) and TPO nonpeptide mimetics (eltrombopag, AKR501) have been shown to increase platelet counts in healthy volunteers and patients with chronic idiopathic thrombocytopenic purpura.[30-33] We recently created a novel TPO receptor activator, NIP-004.[25] NIP-004 is a nonpeptidyl mimetic of TPO and induces colony formation of megakaryocytes from human CD34 hematopoietic cells by activating the human TPO receptor. Interestingly, NIP-004 displays strict species specificity for the human TPO receptor, as the histidine residue in the transmembrane domain of human TPO receptor is critical for NIP-004 to induce intracellular signaling.[25]

In this study, we use human primary megakaryocytes to demonstrate that IFN- inhibits maturation of demarcation membranes and platelet production, but not endomitosis. We also confirm, in a hu-NOG mouse model, that NIP-004 is effective for the treatment of IFN- –induced thrombocytopenia.

Methods

Reagents and cells

Cytokines, including recombinant human IFN- 2b (Imgenex, San Diego, CA), human PEG-IFN- 2b (PEG-Intron; Schering Plough, Kenilworth, NJ), and recombinant human TPO (R&D Systems, Minneapolis, MN) were obtained as indicated. NIP-004 was chemically synthesized at Nissan Chemical Industries (Chiba, Japan).[25] Human bone marrow– and cord blood–derived CD34 cells were purchased from Lonza Walkersville (Walkersville, MD).

CFU assay

CFU-MK assay was performed using a MegaCult-C (StemCell Technologies, Vancouver, BC). A total of 5 10^3 human bone marrow–derived CD34 cells were cultured in collagen-based medium containing rhTPO in combination with rhIFN- 2b, in a CO_2 incubator for 10 days. After fixation, megakaryocytes were visualized with antihuman CD41a antibody using alkaline phosphatase staining. Nuclei were counterstained with Evans blue. Stained colonies were counted under a microscope (BX51; Olympus, Tokyo, Japan), and colonies, including one or more CD41a-positive megakaryocytes more than 100 m in diameter were counted separately.

Proplatelet formation assay

Human bone-marrow-derived CD34 cells were cultured at 10^5 cells/mL in StemSpan serum-free expansion medium (StemCell Technologies) supplemented with 40 g/mL low density lipoprotein and 10 ng/mL TPO at 37°C with 5% CO_2 for 7 days. Megakaryocytes were enriched by velocity sedimentation, as described by Choi et al.[34] Briefly, cultured cells were suspended in CATCH buffer (phosphate-buffered saline with 13.6 mM sodium citrate, 2.2 M prostaglandin E1, 1 mM theophylline, and 1 mM glucose) at 5 10^5 cells/mL and were subjected to a 2-step bovine serum albumin (BSA) gradient, 2.41% (2.5 mL) and 4.83% (5.0 mL), at 1 g for 1.5 hours at room temperature. Large megakaryocytes were collected from the bottom layer and cultured with 10 ng/mL of TPO in combination with 0 to 10 ng/mL of IFN- 2b in 96-well plates for 4 to 6 days. Proplatelet-displaying megakaryocytes were defined as cells that exhibited one or more filament-like protrusions with tips, and were counted under an inverted microscope at a magnification of 200. We counted 500 cells and calculated the percentage of megakaryocytes with proplatelets. Three independent experiments were performed using 3 different donor cells.

Fluorescent images

Human CD34 bone marrow–derived cells were cultured with 10 ng/mL TPO for 7 days. Large megakaryocytes were collected by BSA velocity sedimentation and cultured with 10 ng/mL TPO in combination with 0 or 10 ng/mL IFN- 2b on poly-D-lysine culture slide (BD Biosciences, San Jose, CA) for 5 days. Culture-derived cells were fixed with 1% paraformaldehyde for 15 minutes at room temperature and then permeabilized with 0.2% Triton X-100 for 5 minutes at room temperature. Cells were blocked with 2% fetal bovine serum in phosphate-buffered saline for 1 hour and stained with Alexa Fluor 555-conjugated -tubulin (9F3) antibody (Cell Signaling Technology, Danvers, MA) overnight at 4°C. Images were captured by confocal laser and fluorescence microscopy. Single-photon confocal fluorescence images were collected using a Zeiss LSM510 (Carl Zeiss, Welwyn Garden City, United Kingdom) coupled to an inverted microscope (Zeiss Axiovert 100) equipped with a 63 /1.4 numeric aperture oil objective. Alexa Fluor 555 was excited at 535 nm and emissions were collected above 560 nm.

Real-time quantitative reverse-transcriptase polymerase chain reaction

Total RNA was extracted using a RNeasy Mini Extraction Kit (Qiagen, Hilden, Germany), and 0.5 g of RNA was subjected to reverse transcription using a SuperScript First-Strand Synthesis System for reverse-transcriptase polymerase chain reaction (RT-PCR; Invitrogen, Carlsbad, CA). TaqMan Gene Expression Assays were used for RT-PCR following the manufacturer's instructions. The plate was run on an Applied Biosystems 7500 Fast Real-Time PCR System (Applied Biosystems, Foster, CA). All reactions were normalized with the respective hypoxanthine ribosyl transferase (HPRT) mRNA levels, and experiments were performed in triplicate. HPRT was chosen as an endogenous control from the results using a TaqMan Human Endogenous Control Plate (Applied Biosystems).

In vivo assay

Immunodeficient NOG mice were created at the Central Institute for Experimental Animals (Kawasaki, Kanagawa, Japan) and were maintained under specific pathogen-free conditions.[25] NOG mice were provided with sterile water containing prophylactic neomycin sulfate (Invitrogen). After 2.4 Gy irradiation, 10^5 human umbilical cord blood–derived CD34 cells were intravenously injected into NOG mice. Three months later, PEG-IFN-2b was subcutaneously administered into the NOG mice 3 times weekly for 3 weeks. After we confirmed PEG-IFN- 2b–induced thrombocytopenia, NIP-004 was administered in combination with 30 g/kg PEG-IFN-2b for an additional 4 weeks. The number of human platelets was measured by flow cytometry using species-specific antibodies against human CD41 and Flow-Count Fluorospheres (Beckman Coulter, Fullerton, CA). For measuring the life span of human platelets in hu-NOG mice, in vivo biotinylation was performed as previously described.[35] Briefly, 3 mg sulfo-NHS-LC-biotin (Pierce Chemical, Rockford, IL) was dissolved in 300 L saline, and 150 L of the solution was injected intravenously. Blood from biotinylated mice was stained by antibodies against human CD41a and CD42b and phycoerythrin Texas red (ECD)–labeled streptavidin (BD Biosciences PharMingen, San Diego, CA). Samples were analyzed by flow cytometry to obtain the number of biotinylated human platelets. From plots of the number of biotinylated human platelets vs time, an estimate of the life span was obtained by linear extrapolation. Animal experiments were conducted according to the guidelines for animal experiments[36] of the Japanese Association for Laboratory Animal Science. All experimental protocols were approved by the ethics review committees for animal experiments of Keio University and Nissan Chemical Industries.

Flow cytometry

Multicolor flow cytometry was performed using an EPICS-XL flow cytometer (Beckman Coulter) as previously described.[25] Antibodies used in this study were as follows: antihuman CD33-fluorescein isothiocyanate (FITC), CD3-FITC, CD41a-FITC, CD71-FITC, CD42a-FITC, CD34-phycoerythrin (PE), CD41a-PE, glycophorin A (GPA)-PE, CD42b-PE, CD19-PE, CD45-ECD, CD41a-PE 5 succinimidylester (PC5), CD38-PC5, antimurine CD45-FITC, and CD41-FITC. Antibodies against antihuman

CD45-ECD were purchased from Immunotech (Marseille, France). Other antibodies were purchased from BD Biosciences PharMingen. The actual number of platelets and bone marrow cells in hu-NOG mice and culture-derived platelets was measured by flow cytometry using the indicated species-specific antibodies and Flow-Count Fluorospheres. To analyze human megakaryocyte ploidy, culture-derived cells and bone marrow cells from hu-NOG mice were stained with antihuman CD41a-PE antibody and fixed with 1% paraformaldehyde. Fixed cells were treated with Tween 20 and 7-amino-actinomycin D (7-AAD) dye (Immunotech) followed by 2-color cytometric analysis.

Electron microscopy

Human bone marrow–derived CD34 cells were cultured with 10 ng/mL of TPO for 7 days. Large megakaryocytes were collected by BSA velocity sedimentation and cultured with 10 ng/mL TPO in combination with 0 or 10 ng/mL IFN- 2b and 0 or 1 g/mL NIP-004 for 5 days. Culture-derived cells were fixed in 2% glutaraldehyde in 0.1 M phosphate buffer (pH 7.4) for 60 minutes at 4°C. The samples were washed, then fixed with 1% osmium tetroxide in 0.1 M phosphate buffer for 60 minutes at 4°C, dehydrated with a graded ethanol series, and embedded in Epon (TAAB Laboratories, Aldermaston, United Kingdom), as described previously.[37] Ultrathin sections were prepared, stained with uranyl acetate and lead citrate, and then examined with a JEM1200EX transmission electron microscope (JEOL, Tokyo, Japan) at an accelerating voltage of 80 kV. To evaluate the differentiation of megakaryocytes, we divided megakaryocytes into 3 types according to their developmental stage. We defined immature megakaryocytes, with a large round nucleus but no demarcation membrane system, as type 1 megakaryocytes. Type 2 megakaryocytes were the intermediate stage between types 1 and 3 megakaryocytes. Type 3 were fully matured megakaryocytes, in which the nucleus was pushed to the side of the cell, cytoplasm was abundant, and the area of the demarcation membrane system was more than 20% of the cell body. We counted more than 100 megakaryocytes by electron microscopy and calculated the percentage of each type.

Statistical analysis

Comparisons among groups were performed by Student *t* test. All tests were 2-sided and *P* less than .05 was considered significant.

Results

Colony-forming assay of megakaryocytes using human CD34 hematopoietic stem cells

To investigate how IFN- reduces the number of platelets, we performed colony-forming assays of megakaryocytes using human bone marrow–derived CD34 cells. IFN- 2b at 1 and 10 ng/mL reduced the number of CFU-MK by 13% and 18%, respectively; however, these decreases were not statistically significant (Figure 1A left panel). The average CFU-MK was calculated from 3 independent experiments. We noticed that the size of megakaryocytes treated with IFN- was smaller than that without IFN- ; thus, we counted the number of CFU-MK that included one or more megakaryocytes more than 100 m in diameter. IFN- 2b at 1 and 10 ng/mL significantly reduced the number of CFU-MK that included at least one large megakaryocyte by 42% and 67%, respectively (*P* .05, n 3; Figure 1A right panel).

The effects of IFN- 2b on DNA ploidy of human megakaryocytes in vitro

To investigate whether the reduction of megakaryocyte cell size by IFN- 2b was caused by the inhibition of endomitosis, we measured DNA ploidy of megakaryocytes by flow cytometry.

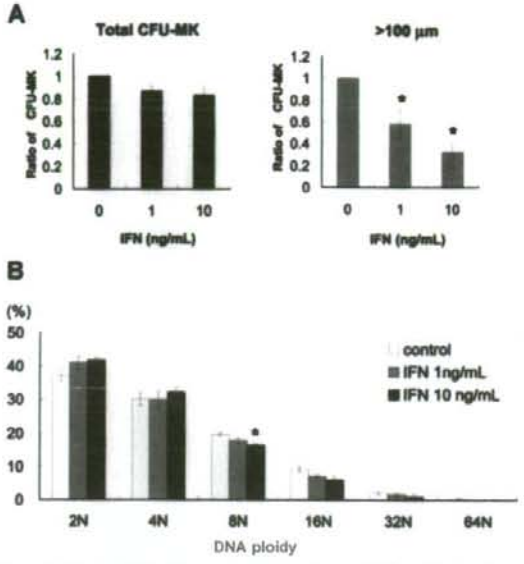

Figure 1. Effects of IFN- 2b on colony formation and DNA ploidy of primary human megakaryocytes. (A) Human bone marrow–derived CD34 cells were treated with 10 ng/mL TPO and 0, 1, or 10 ng/mL IFN- 2b for 10 days. (Left graph) Total number of CFU-MK. The average number was calculated from 3 independent experiments. (Right graph) Number of CFU-MK that included one or more megakaryocytes more than 100 m in diameter. Diameters were measured under a microscope using a microscale within an eyepiece. Data are means plus or minus SEM from the results of 3 independent experiments (**P* .05 vs 0 ng/mL IFN- 2b). (B) Effects of IFN- 2b on DNA ploidy of megakaryocytes in vitro. Human bone marrow–derived CD34 cells were cultured with 10 ng/mL of TPO in combination with 0, 1, or 10 ng/mL IFN- 2b. Megakaryocytes were stained with antihuman CD41a-PE antibody and 7-AAD dye, and examined by 2-color cytometry. Data are means plus or minus SEM from the results of 3 independent experiments (**P* .05 vs 0 ng/mL IFN- 2b).

We cultured human bone marrow–derived CD34 cells with 10 ng/mL of TPO in combination with 0, 1, and 10 ng/mL IFN- 2b for 10 days and analyzed DNA ploidy of megakaryocytes. IFN- 2b did not alter DNA ploidy of human megakaryocytes except 8N with 10 ng/mL IFN- 2b (*P* .05, n 3; Figure 1B). Three independent experiments were performed to confirm reproducibility.

IFN- 2b inhibited platelet production in vitro

As we found that IFN- 2b did not inhibit endomitosis of megakaryocytes, we investigated the effects of IFN- 2b on proplatelet formation (PPF) and platelet production, using primary human megakaryocytes. We defined PPF as megakaryocytes that displayed at least one filament-like extension with tips, and counted 500 cells in 3 independent experiments (Figure 2). IFN- 2b significantly inhibited PPF in a dose-dependent manner (Figure 2A). IFN- 2b at 1 and 10 ng/mL inhibited PPF by 39% and 60%, respectively, on day 12, and by 47% and 61%, respectively, on day 13 (*P* .05, n 3).

We also counted the number of culture-derived platelets by flow cytometry. The platelets produced from primary human megakaryocytes in the culture supernatant were collected and stained with antihuman CD41a and CD42a antibodies. IFN- 2b at 1 and 10 ng/mL reduced the number of culture-derived platelets by 60% and 73%, respectively, on day 13 (*P* .05, n 3; Figure 2B). We performed 3 independent experiments using 3 different donors to

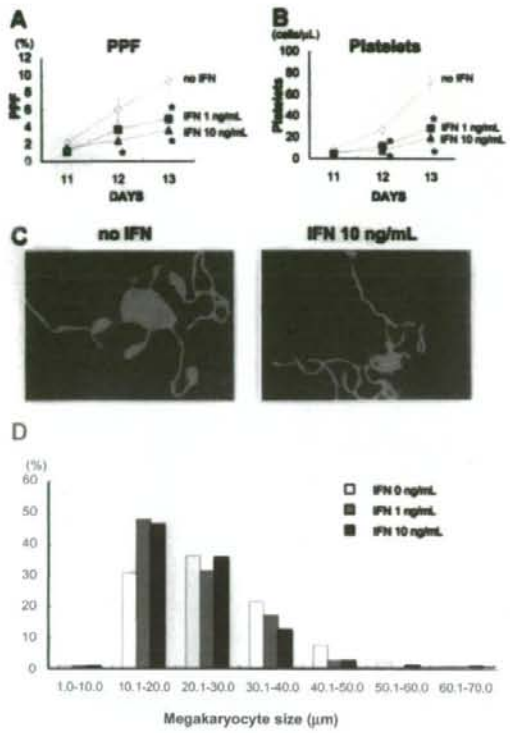

Figure 2. IFN- 2b inhibited proplatelet formation (PPF) and production of platelets from primary human megakaryocytes. Human bone marrow–derived CD34 cells were cultured with 10 ng/mL TPO for 7 days. After collecting large megakaryocytes using velocity sedimentation, we maintained the cells with 10 ng/mL TPO in combination with 10 ng/mL IFN- 2b in 96-well plates for 6 days. (A) The numbers of megakaryocytes displaying PPF were counted under an inverted microscope at 200. We counted 500 cells for each sample 3 times. Data are means plus or minus SEM (n 3). (B) Platelets in the culture supernatant of primary human megakaryocytes were stained with antihuman CD41a and CD42a antibodies and counted by flow cytometry. Data are means plus or minus SEM (n 3). (C) A representative picture of PPF with TPO and TPO plus IFN- 2b. Megakaryocytes were stained with Alexa Fluor 555-conjugated -tubulin (9F3) antibody on day 12 and photographed under confocal laser microscopy. (D) IFN- 2b decreased the size of human megakaryocytes. Megakaryocytes were collected on day 13 and spun down on to glass slides. After staining with Wright-Giemsa solution, the diameters of the megakaryocytes were measured with a microscope using a scale within an eyepiece.

confirm reproducibility. IFN- 2b did not change the appearance of proplatelets, such as branches, shafts, and tips (Figure 2C), although it significantly inhibited the percentage of megakaryocytes demonstrating PPF and the count of culture-derived platelets (Figure 2A,B). Because PPF and the number of platelets reflect the development of the demarcation membrane system in cytoplasm, we measured the size of each megakaryocyte on day 13; these were then cytospun on to glass slides and stained with Giemsa solution (Figure 2D). IFN- 2b at 1 and 10 ng/mL decreased the mean size of human megakaryocytes from 27.3 (0 ng/mL) to 23.5 and 23.7 m, respectively.

IFN- 2b suppressed mRNA expression of transcription factors regulating late-stage megakaryopoiesis

To clarify the molecular mechanism of how IFN- 2b inhibits cytoplasmic maturation and platelet production in megakaryocytes, we analyzed mRNA expression of GATA-1, p45$^{NF\text{-}E2}$, MafG, and VWF using quantitative PCR. The transcription factors GATA-1, p45$^{NF\text{-}E2}$, and MafG are reported to be involved in late-stage megakaropoiesis.[38-40] VWF in -granules is a marker of cytoplasmic maturation of megakaryocytes.[41] We extracted total RNA from human megakaryocytes that were cultured with 10 ng/mL TPO and 0, 1, and 10 ng/mL IFN- 2b for 5 days after BSA-based velocity sedimentation. The mRNA expression of these transcription factors was inhibited by IFN- 2b in a dose-dependent manner (Figure 3). IFN- 2b at 10 ng/mL suppressed the mRNA expression levels of GATA-1, p45$^{NF\text{-}E2}$, MafG, and VWF by 70%, 58%, 55%, and 68%, respectively (Figure 3).

IFN- 2b decreased the number of human platelets without affecting the number and DNA ploidy of human megakaryocytes in hu-NOG mice

To evaluate the effects of human IFN- 2b on human megakaryopoiesis in vivo, we transplanted human umbilical cord blood–derived CD34 cells into NOG mice. We administered PEG-IFN- 2b at 10 and 30 g/kg to hu-NOG mice 3 times weekly for 7 weeks and found that IFN- 2b significantly reduced the number of human platelets by 59% and 68%, respectively, compared with that in the control mice (Figure 4A left panel). The number of murine platelets was not changed by PEG-IFN- 2b because human IFN- 2b does not affect murine cells (Figure 4A right panel). To precisely analyze the effects of PEG-IFN- 2b on human hematopoiesis, we counted the number in each lineage of human hematopoietic cells in bone marrow of hu-NOG mice, using flow cytometry (Table 1). PEG-IFN- 2b at 10 or 30 g/kg 3 times weekly for 7 weeks did not reduce the number of human CD41 megakaryocytes. By contrast, PEG-IFN- 2b significantly reduced the number of human CD45 CD33 myeloid cells and CD45 CD71 GPA erythroblasts in the bone marrow of hu-NOG mice (Table 1). None of the lineages of murine hematopoietic cells was changed by PEG-IFN- 2b (data not shown) because of species specificity. As PEG-IFN- 2b decreased the number of human platelets in hu-NOG mice, we evaluated the effects of PEG-IFN- 2b on endomitosis of human megakaryocytes by flow cytometry. PEG-IFN- 2b had no effects on DNA ploidy of human megakaryocytes in hu-NOG mice (Figure 4B), which was consistent with the data from in vitro experiments.

IFN- did not promote the clearance of human platelets in hu-NOG mice

To exclude the possibility that IFN- may facilitate the clearance of human platelets in hu-NOG mice by activating human platelets or macrophages, we measured the life span of human platelets in hu-NOG mice by labeling them with biotin. When hu-NOG mice were treated with PEG-IFN- 2b 30 g/kg 3 times weekly for 3 weeks, the number of human platelets was decreased by 47%, and the life span of human platelets was 6.1 (0.2) days (mean SEM, n 5). In control hu-NOG mice treated with vehicle, the life span of human platelets was 6.0 (0.2) days (n 4). Because the life span of human platelets was not changed by IFN- 2b treatment, we concluded that IFN- 2b decreased human platelet count by inhibiting platelet production, but not by promoting their clearance.

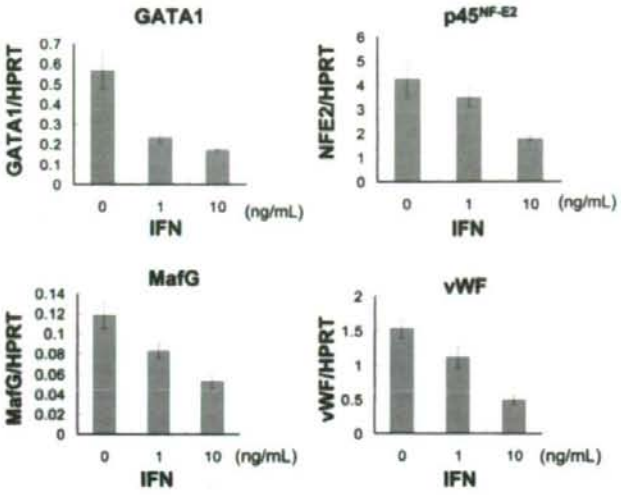

Figure 3. IFN- 2b suppressed expression of transcription factors regulating late-stage megakaryopoiesis. Human bone marrow–derived CD34 cells were incubated with 10 ng/mL TPO for 7 days. Large megakaryocytes were enriched by velocity sedimentation, followed by 6 days of incubation with 10 ng/mL TPO and 0, 1, or 10 ng/mL IFN- 2b. Total RNA was extracted from these megakaryocytes. TaqMan Gene Expression Assay was used for real-time PCR. All data were standardized with respective HPRT mRNA levels. Data are means plus or minus SEM of 3 samples.

NIP-004 was effective for treating IFN- –induced thrombocytopenia in hu-NOG mice

We recently developed a novel nonpeptidyl Mpl activator, NIP-004, that can induce formation of CFU-MK and increase human platelets in hu-NOG mice.[25] To evaluate the effects of NIP-004 on IFN- –induced thrombocytopenia, we administered NIP-004 30 mg/kg per day to hu-NOG mice after 3 weeks of treatment with PEG-IFN- 2b. NIP-004 restored human platelet

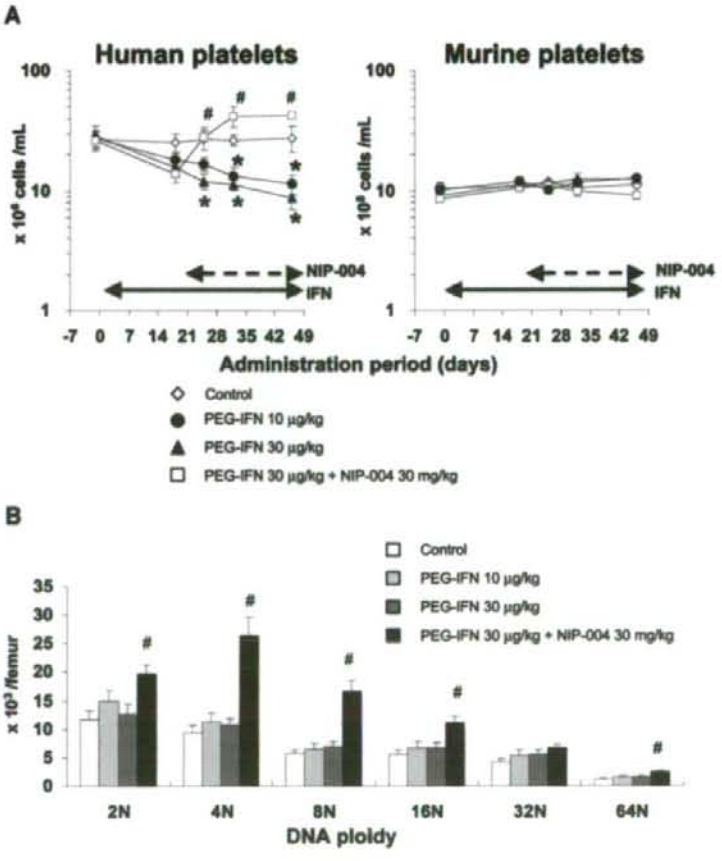

Figure 4. Effects of IFN- 2b and NIP-004 on human platelets and megakaryocytes in hu-NOG mice. Human cord blood–derived CD34 cells were transplanted into immunodeficient NOG mice (hu-NOG). Three months after transplantation, human PEG-IFN- 2b was administered to hu-NOG mice 3 times weekly for 7 weeks. NIP-004 was administered daily to hu-NOG mice for 4 weeks, 3 weeks after initial treatment with PEG-IFN- 2b. (A) The number of human platelets was decreased by PEG-IFN- 2b in a dose-dependent manner. NIP-004 reversed the decrease in human platelets. By contrast, the number of murine platelets in hu-NOG mice was not changed because of the species specificity of human PEG-IFN- 2b and NIP-004. (B) DNA ploidy of human megakaryocytes in hu-NOG mice. Bone marrow cells collected from hu-NOG mice were stained with antihuman CD41a antibody and 7-AAD dye. The number of each ploidy in human megakaryocytes was measured by flow cytometry using Flow-Count Fluorospheres. Data are means plus or minus SEM from 5 mice (*P .05 vs control; #P .05 vs PEG-IFN- 2b 30 g/kg).

Table 1. Cell counts of each human hematopoietic lineage in bone marrow of hu-NOG mice

Lineage	Control, n 5	IFN 10 g/kg, n 5	IFN 30 g/kg, n 5	IFN 30 g/kg; NIP-004 30 mg/kg, n 5
Total white blood cells, 10^6	6.5 0.5	3.9 0.6	4.7 0.7	5.4 0.4
Megakaryocytes, 10^4	3.9 0.5	4.7 0.5	4.7 0.5	8.2 0.6*†
Myeloid cells, 10^6	2.5 0.3	0.9 0.1*	1.0 0.1*	2.0 0.2
Erythroblasts, 10^4	6.9 1.5	1.1 0.5*	0.2 0.1*	0.3 0.1*
Progenitor cells, 10^6	3.2 0.9	3.1 0.5	3.9 0.8	4.4 0.3
B cells, 10^6	3.2 0.3	2.2 0.4	3.0 0.7	2.2 0.2
T cells, 10^6	2.6 0.2	1.6 0.2	1.3 0.3	1.8 0.2

Data are means (SEM) of cells/femur for 5 mice. Bone marrow cells were collected from the femurs of NOG mice transplanted with human umbilical cord blood–derived CD34 cells (hu-NOG). The number in each cell lineage was measured by flow cytometry using lineage-specific antibodies and Flow-Count Fluorospheres. PEG-IFN- 2b and NIP-004 were administered using the same protocol as described in Figure 4. Each lineage-specific marker was indicated as follows: total white blood cells, CD45 ; megakaryocytes, CD41 ; myeloid cells, CD45 CD33 ; erythroblasts, CD45 CD71 GPA ; progenitor cells, CD45 CD34 ; B cells, CD45 CD38 CD19 ; T cells, CD45 CD38 CD3 .

*P .01 versus control.

†P .01 versus PEG-IFN- 2b 30 g/kg single treatment.

counts in hu-NOG mice undergoing treatment with PEG-IFN- 2b 30 g/kg (Figure 4A). NIP-004 30 mg/kg per day significantly increased the number of human megakaryocytes in all DNA ploidy classes but the 32N class with statistically significant differences in hu-NOG mice (Figure 4B; Table 1). NIP-004 did not affect murine megakaryopoiesis because it does not work for murine cells, as previously described (Figure 4A right panel, and data not shown).[25]

IFN- 2b inhibited the development of the demarcation membrane system in human megakaryocytes

To analyze the effects of IFN- 2b on cytoplasmic maturation of human megakaryocytes, ultrastructural study using electron microscopy was performed. When human megakaryocytes were cultured with TPO, almost half the cells had a lobulated nucleus and abundant cytoplasm with a mature demarcation membrane system (Figure 5Avii). The percentages of each type of megakaryocyte were 13% for type 1 (immature; Figure 5Ai), 44% for type 2 (intermediate; Figure 5Aiv), and 43% for type 3 (mature; Figure 5Avii). When megakaryocytes were cultured with TPO and IFN- 2b, the percentages of each type were 12% for type 1 (Figure 5Aii), 63% for type 2 (Figure 5Av), and 25% for type 3 (Figure 5Aviii). The percentage of type 3 megakaryocytes was reduced by 42% and type 2 was increased by 43% with IFN- 2b compared with controls (Figure 5B). For each type, we observed no obvious effects of IFN- 2b on the number of granules or the appearance of mitochondria and nuclei. We performed 4 experiments separately to confirm reproducibility and to calculate the average and standard deviation (Figure 5B). These results indicated that IFN- 2b inhibited the maturation of the demarcation membrane system in primary human megakaryocytes. Next, we tested whether NIP-004 inhibited the effects of IFN- 2b on the maturation of the demarcation membrane system. When megakaryocytes were cultured with TPO plus IFN- 2b plus NIP-004, the percentages of each type were 7% for type 1 (Figure 5Aiii), 46% for type 2 (Figure 5Avi), and 47% for type 3 (Figure 5Aix). These results indicated that NIP-004 prevented the inhibitory effects of IFN- 2b on the maturation of the demarcation membrane system in primary human megakaryocytes (Figure 5B). We performed 2 experiments separately to confirm reproducibility (P .05).

Discussion

IFN- has been proposed to induce thrombocytopenia mainly by inhibiting proliferation and maturation of megakaryocytes.[12-15] Autoimmune-based destruction of platelets[20,21] and capillary sequestration have also been proposed as causes of IFN- -induced thrombocytopenia.[18,20-22] In this study, we used primary human megakaryocytes to successfully demonstrate that IFN- 2b inhibited cytoplasmic maturation and platelet production of megakaryocytes, but not proliferation and endomitosis. Leukemia cell lines do not demonstrate PPF or produce platelets; thus, in this study, we used human primary megakaryocytes for in vitro assays and in vivo models to analyze the mechanism of IFN-induced thrombocytopenia.

Because IFN- 2b did not decrease the number of CFU-MK using human CD34 cells, we speculate that IFN- 2b does not inhibit the commitment of CD34 cells to the megakaryocytic lineage and proliferation of immature megakaryocytes, but it does inhibit late-stage megakaryopoiesis. PPF and platelet production represent late-stage megakaryopoiesis; therefore, we used human primary megakaryocytes to analyze the effects of IFN- 2b on PPF and platelet production. As expected, IFN- 2b significantly inhibited PPF and platelet production in vitro. We also evaluated cytoplasmic maturation of megakaryocytes by electron microscopy. IFN- 2b reduced by half the percentage of type 3 megakaryocytes with a fully matured demarcation membrane system. This result suggested that IFN- 2b inhibited maturation of the demarcation membrane system in megakaryocytes. Demarcation membranes are thought to be the membrane reservoir for formation of proplatelets. The precise molecular mechanisms of how IFN- 2b inhibits the maturation of demarcation membranes and platelet formation remain to be elucidated. Inhibition of maturation of the demarcation membrane system by IFN- 2b may be involved in the impairment of PPF. This might affect the inhibition of PPF and platelet production.

IFN- 2b did not reduce the number of human megakaryocytes, although it significantly reduced the number of human platelets in hu-NOG mice. As well, IFN- 2b did not alter DNA ploidy of human megakaryocytes in the bone marrow of hu-NOG mice, indicating that IFN- 2b inhibited late-stage megakaryopoiesis. Previous clinical studies have demonstrated that IFN- reduces the

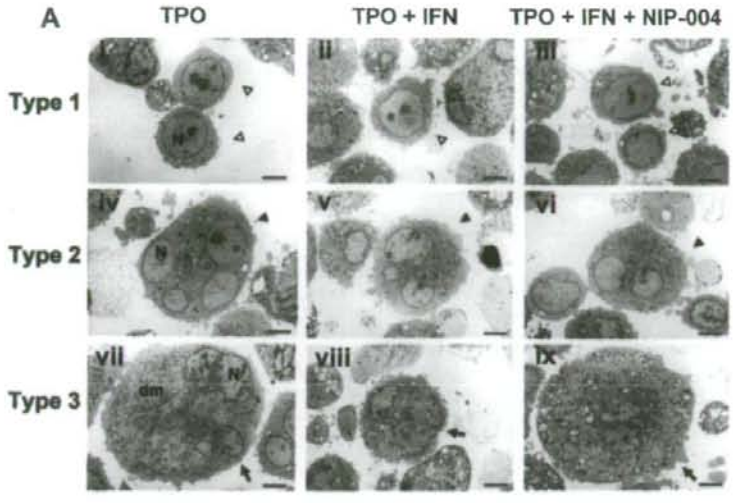

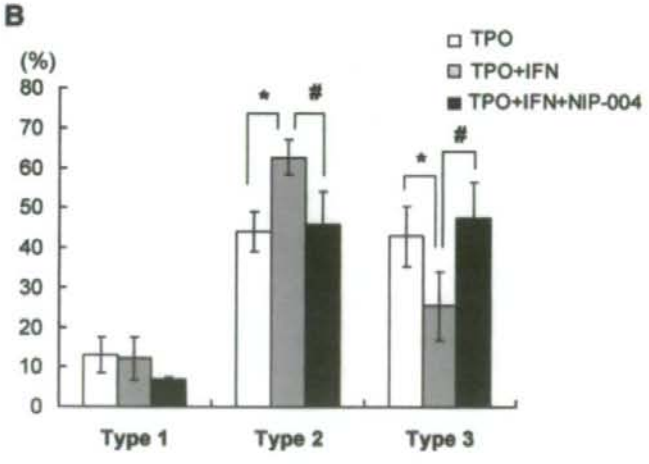

Figure 5. Ultrastructure of megakaryocytes cultured with or without IFN- 2b. (A) Ultrastructures of representative human megakaryocytes cultured with 10 ng/mL TPO, 10 ng/mL TPO plus 10 ng/mL IFN- 2b, and 10 ng/mL TPO plus 10 ng/mL IFN- 2b plus 1 g/mL NIP-004. represent type 1 immature megakaryocytes (i-iii); Š, type 2 intermediate megakaryocytes (iv-vi); →, type 3 fully matured megakaryocytes (vii-ix). The definition of each type is in "Electron microscopy." Original magnification, 3000. Scale bar represents 4 m. N indicates nucleus; Dm, demarcation membranes. (B) The percentage of each type of megakaryocytes. IFN- 2b decreased type 3 megakaryocytes and increased type 2 compared with control (TPO) with statistically significant differences, indicating that IFN- 2b inhibits the development of the demarcation membrane system of megakaryocytes. Data are means plus or minus SD from the results of 4 independent experiments (*P .05 vs TPO). NIP-004 prevented the inhibitory effects of IFN- 2b on the development of the demarcation membrane system of megakaryocytes. Data are means plus or minus SD from the results of 2 independent experiments (#P .05 vs TPO IFN).

number of platelets without decreasing the number of megakaryocytes in patients with chronic hepatitis, solid tumors, and myeloproliferative disorders,[16-19] which is consistent with our results. IFN- has been reported to significantly decrease the size of megakaryocytes in patients with essential thrombocythemia and polycythemia vera.[17,19] These clinical observations also support our conclusion that IFN- inhibits cytoplasmic maturation of megakaryocytes but not endomitosis.

Because it is possible that IFN- promotes the consumption of platelets in hu-NOG mice, we measured the life span of human platelets in hu-NOG mice and found that IFN- 2b did not shorten the life span. Therefore, we concluded that IFN- 2b induced thrombocytopenia by inhibiting platelet production, but not by facilitating the consumption of platelets. GATA-1 and NF-E2 are essential transcription factors in late-stage megakaryopoiesis. Lineage-selective GATA-1 knockout mice have abnormal megakaryocytes with a small cytoplasm and few granules.[38] GATA-1 knockdown megakaryocytes are small, with low ploidy.[42] NF-E2 is composed of 2 basic leucine zipper subunits of $p45^{NF-E2}$ and p18 and is one of the small Maf proteins that includes MafG.[43] $p45^{NF-E2}$ knockout megakaryocytes do not have platelet formation and granules, but their DNA ploidy is increased in compensation.[40] MafG-null mutant mice exhibit thrombocytopenia and impairment of PPF.[39,44] We demonstrated that IFN- 2b suppressed mRNA expression levels of GATA-1, $p45^{NF-E2}$, and MafG in primary human megakaryocytes using quantitative PCR. Down-regulation of these transcription factors might be involved in inhibition of the cytoplasmic maturation of human megakaryocytes by IFN- . Ishida et al used murine megakaryocytes and reported that limitin and IFN- induce the expression of Daxx protein and phosphorylation of Crk adaptor protein.[45] IFN- –induced growth inhibition is also mediated by Crk in myeloid and erythroid progenitor cells, and by Daxx in B lymphoid progenitors.[46,47] Wang et al demonstrated that IFN- induces the expression of SOCS-1 transcription factor, which could blunt TPO-induced intracellular signaling in murine primary megakaryocytes.[12] IFN- activates JAK1 and TYK2 tyrosine kinses, which phosphorylate STAT1 and STAT2 transcription factors. Phosphorylated STAT1 and STAT2 form a complex

with IFN regulatory factor (IRF)-9, named IFN-stimulating gene factor 3. IFN-stimulating gene factor 3 migrates into the nucleus where it binds to the IFN-stimulated response element in the promoter region of hundreds of genes. STAT1/STAT1 homodimer mediates the alternative pathway by binding to IFN- activated sequence. To the best of our knowledge, no other study has demonstrated how IFN- decreases the expression of GATA-1, $p45^{NF\text{-}E2}$, and MafG. Further investigation will be needed to elucidate this mechanism.

NIP-004 is a novel TPO mimetic and can increase the number of human megakaryocytes and induce their maturation, accompanied by an increase in human platelets in hu-NOG mice.[25] We confirmed the effects of NIP-004 on IFN- -induced thrombocytopenia using hu-NOG mice in this study. NIP-004 increased the number of human megakaryocytes in hu-NOG mice treated with IFN- 2b. The dose of PEG-IFN- 2b in this study was higher than that used in clinical settings. Based on our preliminary data related to the pharmacokinetics of PEG-IFN- 2b in NOG mice, we found that clearance of PEG-IFN- 2b was 3 times faster than that in humans (data not shown). Therefore, we needed to inject PEG-IFN- 2b at higher doses to retain an effective concentration in NOG mice.

In conclusion, we demonstrated that IFN- 2b directly inhibited cytoplasmic maturation and platelet production, but not proliferation and endomitosis in human primary megakaryocytes. TPO mimetics might be useful for treating IFN-induced thrombocytopenia, and their clinical application might encourage physicians and patients to continue IFN therapy.

Acknowledgments

The authors thank Ms Asako Ikejima for technical assistance, Dr Kenneth Kaushansky for encouragement, and Dr Eri Matsuki for discussions.

Authorship

Contribution: A.Y. and T.N. performed the experiments, analyzed results, and compiled the figures; H.S. performed electron microscopy; M.I. and Y.O. contributed live mice; Y.I. controlled the data; and A.Y., T.N., and Y.M. designed the research and wrote the paper.

Conflict-of-interest disclosure: T.N. is an employee of Nissan Chemical Industries. Y.M. and Y.O. received research grants from Nissan Chemical Industries. The remaining authors declare no competing financial interests.

Correspondence: Yoshitaka Miyakawa, Division of Hematology, Department of Internal Medicine, Keio University School of Medicine, 35 Shinanomachi, Shinjuku, Tokyo 160-8582, Japan; e-mail: yoshi@sc.itc.keio.ac.jp.

References

1. Manns MP, McHutchison JG, Gordon SC, et al. Peginterferon alfa-2b plus ribavirin compared with interferon alfa-2b plus ribavirin for initial treatment of chronic hepatitis C: a randomized trial. Lancet. 2001;358:958-965.
2. Fried MW, Shiffman ML, Reddy KR, et al. Peginterferon alfa-2a plus ribavirin for chronic hepatitis C virus infection. N Engl J Med. 2002;347:975-982.
3. Tremolada F, Casarin C, Alberti A, et al. Long-term follow-up of non-A, non-B (type C) post-transfusion hepatitis. J Hepatol. 1992;16:273-281.
4. Fattovich G, Giustina G, Degos F, et al. Morbidity and mortality in compensated cirrhosis type C: a retrospective follow-up study of 384 patients. Gastroenterology. 1997;112:463-472.
5. Hu K-Q, Tong MJ. The long-term outcomes of patients with compensated hepatitis C virus-related cirrhosis and history of parenteral exposure in the United States. Hepatology. 1999;29:1311-1316.
6. Heathcote EJ, Shiffman ML, Cooksley WG, et al. Peginterferon alfa-2a in patients with chronic hepatitis C and cirrhosis. N Engl J Med. 2000;343:1673-1680.
7. Horoldt B, Haydon G, O'Donnell K, Dudley T, Nightingale P, Mutimer D. Results of combination treatment with pegylated interferon and ribavirin in cirrhotic patients with hepatitis C infection. Liver Int. 2006;26:650-659.
8. Helbling B, Jochum W, Stamenic I, et al. HCV-related advanced fibrosis/cirrhosis: randomized controlled trial of pegylated interferon -1a and ribavirin. J Viral Hepat. 2006;13:762-769.
9. Hofer H, Gurguta C, Bergholz U, Steindl-Munda P, Ferenci P. Standard interferon-alpha in combination with ribavirin for hepatitis C patients with advanced liver disease and thrombocytopenia. Wien Klin Wochenschr. 2006;118:595-600.
10. Shiffman ML, Bisciglie AMD, Lindsay KL, et al. Peginterferon alfa-2a and ribavirin in patients with chronic hepatitis C who have failed prior treatment. Gastroenterology. 2004;126:1015-1023.
11. Nishiguchi S, Kuroki T, Nakatani S, et al. Randomised trial of effects of interferon-alpha on incidence of hapatocellular carcinoma in chronic active hepatitis C with cirrhosis. Lancet. 1995;346:1051-1055.
12. Wang Q, Miyakawa Y, Fox N, Kaushansky K. Interferon-alpha directly represses megakaryopoiesis by inhibiting thrombopoietin-induced signaling through induction of SOCS-1. Blood. 2000;96:2093-2099.
13. Ganser A, Carlo-Stella C, Greher J, Völkers B, Hoelzer D. Effect of recombinant interferons alpha and gamma on human bone marrow-derived megakaryocytic progenitor cells. Blood. 1987;70:1173-1179.
14. Dukes PP, Izadi P, Jorge OA, Shore NA, Gomperts E. Inhibitory effects of interferon on mouse megakaryocytic progenitor cells in culture. Exp Hematol. 1980;8:1048-1056.
15. Mazur EM, Richtsmeier WJ, South K. Alpha-interferon: differential suppression of colony growth from human erythroid, myeloid, and megakaryocytic hematopoietic progenitor cells. J Interferon Res. 1986;6:199-206.
16. Ernstoff MS, Kirkwood JM. Changes in the bone marrow of cancer patients treated with recombinant interferon alpha-2. Am J Med. 1984;76:593-596.
17. Wadenvik H, Kutti J, Ridell B, et al. The effect of -interferon on bone marrow megakaryocytes and platelet production rate in essential thrombocythemia. Blood. 1991;77:2103-2108.
18. Sata M, Yano Y, Yoshiyama Y, et al. Mechanisms of thrombocytopenia induced by interferon therapy for chronic hepatitis B. J Gastroenterol. 1997;32:206-210.
19. Kreft A, Nolde C, Büsche G, Buhr T, Kreipe H, Georgii A. Polycythaemia vera: bone marrow histopathology under treatment with interferon, hydroxyurea and busulphan. Eur Haematol. 2000;64:32-41.
20. Dourakis SP, Deutsch M, Hadziyannis SJ. Immune thrombocytopenia and alpha-interferon therapy. J Hepatol. 1996;25:972-975.
21. Elefsiniotis IS, Pantazis KD, Fotos NV, Moulakakis A, Mavrogiannis C. Late onset autoimmune thrombocytopenia associated with pegylated interferon- -2b plus ribavirin treatment for chronic hepatitis C. J Gastroenterol Hepatol. 2006;21:622-623.
22. Dormann H, Krebs S, Muth-Selbach U, et al. Rapid onset of hematotoxic effects after interferon alpha in hepatitis C. J Hepatol. 2000;32:1041-1042.
23. Odell TT, Jackson C. Polyploidy and maturation of rat megakaryocytes. Blood. 1968;32:102-110.
24. Raslova H, Kauffmann A, Sekkai D, et al. Interrelation between polyploidization and megakaryocyte differentiation: a gene profiling approach. Blood. 2007;109:3225-3234.
25. Nakamura T, Miyakawa Y, Miyamura A, et al. A novel nonpeptidyl human c-Mpl activator stimulates human megakaryopoiesis and thrombopoiesis. Blood. 2006;107:4300-4307.
26. Kaushansky K, Broudy VC, Lin N, et al. Thrombopoietin, the Mpl ligand, is essential for full megakaryocyte development. Proc Natl Acad Sci U S A. 1995;92:3234-3238.
27. Gurney AL, Carver-Moore K, de Sauvage FJ, Moore MW. Thrombocytopenia in c-mpl-deficient mice. Science. 1994;265:1445-1447.
28. Li J, Yang C, Xia Y, et al. Thrombocytopenia caused by the development of antibodies to thrombopoietin. Blood. 2001;98:3241-3248.
29. Basser RL, O'Flaherty E, Green M, Edmonds M, Nichol J, Menchaca DM. Development of pancytopenia with neutralizing antibodies to thrombopoietin after multicycle chemotherapy supported by megakaryocyte growth and development factor. Blood. 2002;99:2599-2602.
30. Kuter DJ. New thrombopoietic growth factors. Blood. 2007;109:4607-4616.
31. Bussel JB, Kuter DJ, Phil D, et al. AMG 531, a thrombopoiesis stimulating protein, for chronic ITP. N Engl J Med. 2006;355:1672-1681.
32. Bussel J, Cheng G, Saleh M, et al. Analysis of bleeding in patients with immune thrombocytopenic purpura (ITP): a randomized, double-blind, placebo-controlled trial of eltrombopag, an oral platelet growth factor [abstract]. Blood. 2006;108:475.

33. Desjardins RE, Tempel DL, Lucker R, Kuter DJ. Single and multiple oral doses of AKR-501 (YM477) increase the platelet count in healthy volunteers [abstract]. Blood. 2006;108:477.
34. Choi ES, Nichol JL, Hokom MM, Hornkohl AC, Hunt P. Platelets generated in vitro from proplatelet-displaying human megakaryocytes are functional. Blood. 1995;85:402-413.
35. Ault KA, Knowles C. In vivo biotinylation demonstrates that reticulated platelets are the youngest platelets in circulation. Exp Hematol. 1995;23:996-1001.
36. Guideline for animal experimentation [in Japanese]. Exp Anim. 1987;36:285-288.
37. Suzuki H, Tanoue K, Yamazaki H. Endocytosis by platelets during cationized ferritin-induced aggregation. Cell Tissue Res. 1985;240:513-517.
38. Shivdasani RA, Fujiwara Y, McDevitt MA, Orkin SH. A lineage-selective knockout establishes the critical role of transcription factor GATA-1 in megakaryocyte growth and platelet development. EMBO J. 1997;16:3965-3974.
39. Shavit JA, Motohashi H, Onodera K, Akasaka J, Yamamoto M, Engel JD. Impaired megakaryopoiesis and behavioral defects in mafG-null mutant mice. Genes Dev. 1998;12:2164-2174.
40. Shivdasani RA, Rosenblatt MF, Zucker-Franklin D, et al. Transcription factor NF-E2 is required for platelet formation independent of the actions of thrombopoietin/MGDF in megakaryocyte development. Cell. 1995;81:695-704.
41. Cramer EM, Debili N, Martin JF, et al. Uncoordinated expression of fibrinogen compared with thrombosporidin and von Willebrand factor in maturing human megakaryocytes. Blood. 1989;73:1123-1129.
42. Muntean AG, Pang L, Poncz M, Dowdy SF, Blobel GA, Crispino JD. Cyclin D-Cdk4 is regulated by GATA-1 and required for megakaryocyte growth and polyploidization. Blood. 2007;109:5199-5207.
43. Igarashi K, Kataoka K, Itoh K, Hayashi N, Nishizawa M, Yamamoto M. Regulation of transcription by dimerization of erythroid factor NF-E2 p45 with small Maf proteins. Nature. 1994;367:568-572.
44. Onodera K, Shavit JA, Motohashi H, Yamamoto M, Engel JD. Perinatal synthetic lethality and hematopoietic defects in compound mafG::mafK mutant mice. EMBO J. 2000;19:1335-1345.
45. Ishida N, Oritani K, Shiraga M, et al. Differential effects of a novel IFN-zeta/limitin and IFN-alpha on signals for Daxx induction and Crk phosphorylation that couple with growth control of megakaryocytes. Exp Hematol. 2005;33:495-503.
46. Platanias LC, Uddin S, Bruno E, et al. CrkL and CrkII participate in the generation of the growth inhibitory effects of interferons on primary hematopoietic progenitors. Exp Hematol. 1999;27:1315-1321.
47. Gongora R, Stephan RP, Zhang Z, Cooper MD. An essential role for Daxx in the inhibition of B lymphopoiesis by type I interferons. Immunity. 2001;14:727-737.

A New Humanized Mouse Model of Epstein-Barr Virus Infection That Reproduces Persistent Infection, Lymphoproliferative Disorder, and Cell-Mediated and Humoral Immune Responses

Misako Yajima,[1,a] Ken-ichi Imadome,[1,a] Atsuko Nakagawa,[2] Satoru Watanabe,[3] Kazuo Terashima,[4] Hiroyuki Nakamura,[1] Mamoru Ito,[6] Norio Shimizu,[3] Mitsuo Honda,[5] Naoki Yamamoto,[4,5] and Shigeyoshi Fujiwara[1]

[1]Department of Infectious Diseases, National Research Institute for Child Health and Development, [2]Pathology Laboratory, Department of Clinical Laboratory Medicine, National Center for Child Health and Development, [3]Department of Virology, Division of Medical Science, Medical Research Institute, and [4]Department of Molecular Virology, Graduate School of Medicine, Tokyo Medical and Dental University, and [5]AIDS Research Center, National Institute of Infectious Diseases, Tokyo, and [6]Central Institute for Experimental Animals, Kawasaki, Japan

The functional human immune system, including T, B, and natural killer lymphocytes, is reconstituted in NOD/Shi-*scid*/IL-2Rγ^{null} (NOG) mice that receive hematopoietic stem cell transplants. Here, we show that these humanized mice can recapitulate key aspects of Epstein-Barr virus (EBV) infection in humans. Inoculation with $\sim 1 \times 10^3$ TD_{50} (50% transforming dose) of EBV caused B cell lymphoproliferative disorder, with histopathological findings and latent EBV gene expression remarkably similar to that in immunocompromised patients. Inoculation with a low dose of virus ($\leqq 1 \times 10^1$ TD_{50}), in contrast, resulted in apparently asymptomatic persistent infection. Levels of activated $CD8^+$ T cells increased dramatically in the peripheral blood of infected mice, and enzyme-linked immunospot assay and flow cytometry demonstrated an EBV-specific T cell response. Immunoglobulin M antibody specific to the EBV-encoded protein BFRF3 was detected in serum from infected mice. The NOG mouse is the most comprehensive small-animal model of EBV infection described to date and should facilitate studies of the pathogenesis, prevention, and treatment of EBV infection.

Epstein-Barr virus (EBV) is a tumor virus associated with a variety of malignancies, including Burkitt lymphoma, nasopharyngeal carcinoma, and Hodgkin lymphoma [1]. It is also an etiological agent of infectious mononucleosis (IM), which is characterized by transient proliferation of EBV-infected B lymphoblastoid cells and an excessive anti-EBV T cell response. EBV has a unique ability to growth transform human B lymphocytes in vitro and establish lymphoblastoid cell lines (LCLs) [2]. EBV-transformed lymphoblasts express 6 nuclear proteins (Epstein-Barr nuclear antigen [EBNA] 1, 2, 3A, 3B, 3C, and LP) and 3 membrane proteins (latent membrane protein [LMP] 1, 2A, and 2B), and this pattern of EBV gene expression is termed latency III. In contrast, Burkitt lymphoma cells express only EBNA1 consistently (latency I), whereas Hodgkin lymphoma and nasopharyngeal carcinoma cells express EBNA1, LMP1, and LMP2 (latency II). In vivo, EBV-transformed cells are effectively removed by virus-specific cytotoxic T cells, and EBV infection in immunocompetent humans is usually subclinical, except for IM caused by primary infection during adolescence or adulthood. However, in immunocompromised hosts, such as patients with AIDS and transplant recipients, EBV-infected B lymphoblasts can proliferate and cause lymphoproliferative disorder.

Received 28 December 2007; accepted 19 March 2008; electronically published 15 July 2008.

Potential conflicts of interest: none reported.

Financial support: Ministry of Health, Labour, and Welfare of Japan (grants H18-Shinko-013 and H19-AIDS-003).

[a] M.Y. and K.-I.I. contributed equally to this study.

Reprints or correspondence: Dr. Shigeyoshi Fujiwara, Dept. of Infectious Diseases, National Research Institute for Child Health and Development, 2-10-1 Okura, Setagaya-ku, Tokyo 157-8535, Japan (shige@nch.go.jp); or, Dr. Norio Shimizu, Dept. of Virology, Div. of Medical Science, Medical Research Institute, Tokyo Medical and Dental University, 1-5-45 Yushima, Bunkyo-ku, Tokyo 113-8519, Japan (nshivir@tmd.ac.jp); or, Dr. Naoki Yamamoto, AIDS Research Center, National Institute of Infectious Diseases, 1-23-1 Toyama, Shinjuku-ku, Tokyo 162-8640, Japan (nyama@nih.go.jp).

The Journal of Infectious Diseases 2008; 198:673–82

0022-1899/2008/19805-0008$15.00
DOI: 10.1086/590502

EBV infects only humans in nature and limited animal species under experimental conditions. It can infect cotton-top tamarins and induce lymphomas, which have been used as a model of EBV-associated lymphomas [3, 4]. Nonhuman primates possess their own lymphocryptoviruses related to EBV, and research on the use of these virus-host systems as models of EBV infection is currently in progress [5, 6]. Small-animal models of EBV have also been developed, which are particularly useful when a large number of animals are necessary. *Scid* mice that receive intraperitoneal transplants of EBV-transformed LCLs or peripheral blood mononuclear cells (PBMCs) isolated from EBV-infected persons develop lymphomas, which have been used as a model of human lymphoproliferative disorder [7–9]. Recently, NOD/*scid* mice transplanted with human hematopoietic stem cells (HSCs) and reconstituted mainly with B lymphocytes were infected with EBV, and the development of lymphoproliferative disorder was described [10]. The immune response to EBV was not studied in these *scid* or NOD/*scid* mouse models. Very recently, a functional human immune system could be reconstituted in highly immunodeficient mouse strains, and these so-called humanized mice were shown able to mount an EBV-specific T cell response [11, 12]. These studies were, however, performed mainly using immunological standpoints and did not provide detailed virological data.

NOD/Shi-*scid*/IL-2Rγ^{null} (referred to here as NOG) is a highly immunodeficient mouse strain that was developed very recently and that, after transplantation with cord blood HSCs, is able to reconstitute most major components of the hematolymphoid system, including T cells, B cells, NK cells, macrophages, and dendritic cells [13–15]. Human T cells that develop in NOG mice are functional in that they can be activated to display cytotoxic activity [15, 16]. These properties made NOG mice an excellent model of human virus infections targeting the immune system, such as those with human T-lymphotropic virus–1 and HIV-1 [17–20]. Here, we provide evidence that humanized NOG mice can reproduce various key aspects of human EBV infection and propose that they may be a valuable tool for studies of EBV infection.

Table 1. Primers for reverse-transcription polymerase chain reaction to detect Epstein-Barr virus (EBV) transcripts.

Transcript, primer	Sequence (5'→3')
EBNA1	
5'	gatgagcgtttgggagagctgattctgca
3'	tcctcgtccatggttatcac
EBNA2	
5'	agaggaggtggtaagcggttc
3'	tgacgggtttccaagactatcc
LMP1	
5'	ctctccttctcctcctcttg
3'	caggagggtgatcatcagta
LMP2A	
5'	atgactcatctcaacacata
3'	catgttaggcaaattgcaaa
LMP2B	
5'	cagtgtaatctgcacaaaga
3'	catgttaggcaaattgcaaa
EBER1	
5'	agcacctacgctgccctaga
3'	aaaacatgcggaccaccagc
BZLF1 (first)	
5'	attgcaccttgccgccaccttg
3'	cgcattttctggaagccacccga
BZLF1 (second)	
5'	gaccaagctaccagagtctat
3'	cagaatcgcattcctccagcga
BMRF1	
5'	ctagccgtcctgtccaagtgc
3'	agccaaacagctccttgccca
BLLF1	
5'	gtcagtacaccatccagagcc
3'	ttggtagacagccttcgtatg
GAPDH	
5'	gcctcctgcaccaccaactg
3'	cgacgcctgcttcaccaccctct

NOTE. EBNA, Epstein-Barr nuclear antigen; EBER, EBV-encoded small RNA; LMP, latent membrane protein.

METHODS

Preparation of humanized mice. NOG mice were obtained from the Central Institute for Experimental Animals (Kawasaki, Japan). Protocols for experiments with NOG mice were approved by the Institutional Animal Care and Use Committee of the National Institute of Infectious Diseases (NIID). Cord blood was supplied by the Tokyo Cord Blood Bank after obtaining informed consent. The use of human materials in this research was approved by the institutional review boards of the National Research Institute for Child Health and Development, the NIID, the Tokyo Medical and Dental University, and the Tokyo Cord Blood Bank. The isolation of human $CD34^+$ HSCs from cord blood by means of the MACS Direct CD34 Progenitor Cell Isolation Kit (Miltenyi Biotec), their intravenous injection (1×10^4 to 1.2×10^5 cells/mouse) into 6–10-week-old female NOG mice, and the characterization of the reconstitution of the human hematoimmune system were done as described elsewhere [18, 20]. NOG mice in which the human hematoimmune system was reconstituted are referred here as humanized NOG (hNOG) mice.

Experimental EBV infection, quantification of viral DNA, and detection of viral mRNAs. Virus production by EBV-infected Akata cells was stimulated by brief treatment with anti-IgG antibody (Dako), and culture fluid was used as inoculum after filtration through a 0.45-μm membrane filter [21]. For virus titration, cord blood lymphocytes were plated at the density

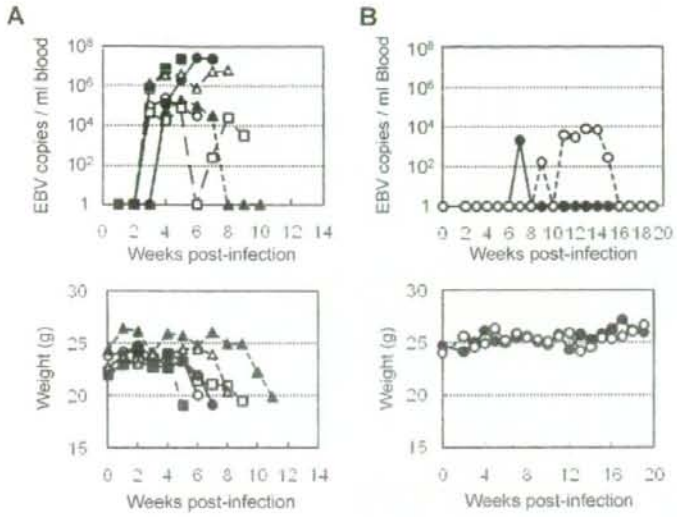

Figure 1. Peripheral blood Epstein-Barr virus (EBV) DNA load and body weight in humanized NOG (hNOG) mice infected with EBV. *A*, Infection at a high dose of virus. Six mice were inoculated intravenously with 1×10^3 TD_{50} of EBV. Peripheral blood EBV DNA load *(upper panels)* and body weight *(lower panels)* were then determined weekly. Each symbol in the graphs represents an individual mouse. Interruption of records indicates the death or killing of a mouse. *B*, Infection at lower doses. Peripheral blood EBV DNA load *(upper panel)* and body weight *(lower panel)* of 2 mice inoculated with low doses of EBV (*black circle*, 1×10^{-1} TD_{50}; *white circle*, 1×10^1 TD_{50}) are shown.

of 2×10^5 cells per well in 6-well plates and then inoculated with serial 10-fold dilutions of virus preparation. The number of wells with proliferating lymphocytes was counted 6 weeks after infection, and the titer of the virus in 50% transforming dose (TD_{50}) was determined by the Reed-Muench method [22]. EBV was inoculated intravenously through the tail vein. EBV DNA was quantified by a real-time quantitative polymerase chain reaction (PCR) assay based on the TaqMan system (Applied Biosystems), as described elsewhere [23]. Analysis of EBV gene expression by reverse-transcription PCR (RT-PCR) was done as described elsewhere, using the primers listed in table 1 [24].

Histopathology, in situ hybridization (ISH), and immunohistochemistry. Tissue samples were fixed in 10% buffered formalin, embedded in paraffin, and stained with hematoxylin-eosin. For phenotypic analysis of proliferating lymphocytes, immunostaining for CD3 (Nichirei), CD4 (Novocastra), CD8 (Nichirei), CD45RO, CD20, CD79a, CD30, Mum1 (Dako), CD23, CD10, CD56 (Novocastra), granzyme B (Dako), and T cell intracellular antigen 1 (Beckman Coulter) was performed on paraffin sections. EBV was detected by immunostaining for LMP1 and EBNA2 (Dako) and by ISH with EBV-encoded small RNA (EBER) probe. Immunohistochemistry and ISH were performed on an automated stainer (Benchmark XT; Ventana Medical Systems), in accordance with the manufacturer's recommendations. To determine the cell lineage of EBV-infected cells, paraffin sections were applied to double staining with EBER ISH and immunohistochemistry.

Detection of EBV-specific T cell response. Enzyme-linked immunospot (ELISPOT) assay was performed with the Immunocyto IFN-γ ELISPOT Kit (MBL), in accordance with the instructions supplied by the manufacturer. Briefly, $CD8^+$ T cells were isolated from PBMCs from EBV-infected hNOG mice with the IMag anti-human CD8 Particles–DM (BD Biosciences). Mixture of these $CD8^+$ T cells and an autologous LCL were incubated with interleukin (IL)–2 in microplates coated with antibody to interferon (IFN)–γ for 17 h. Captured IFN-γ was detected by use of biotinated antibody to IFN-γ and alkaline phosphatase–conjugated streptavidin and was visualized by reaction with the BCIP/NBT chromogen substrate. The unpaired Student's *t* test was used for statistical analysis. IFN-γ secretion in response to EBV was also examined by flow cytometry, as described elsewhere [25]. Briefly, aliquots of murine splenocytes and an LCL were mixed in 6-well plates in the presence of brefeldin A (10 μg/mL) and incubated at 37°C in 5% CO_2 for 17 h. After incubation, the cell suspensions were stained with phycoerythrin-conjugated anti-human CD69, phycoerythrin–Texas red–conjugated anti-human CD45, and phycoerythrin–cyanin 5–conjugated anti-human CD8 for 30 min at 4°C and were fixed with 2% paraformaldehyde. Cells were then permeabilized and stained with BD Perm/Wash buffer (BD Biosciences) containing fluorescein isothiocyanate–conjugated anti-human IFN-γ for 30 min at 4°C. Stained cells were analyzed using an EpicsXL flow cytometer (Beckman Coulter).

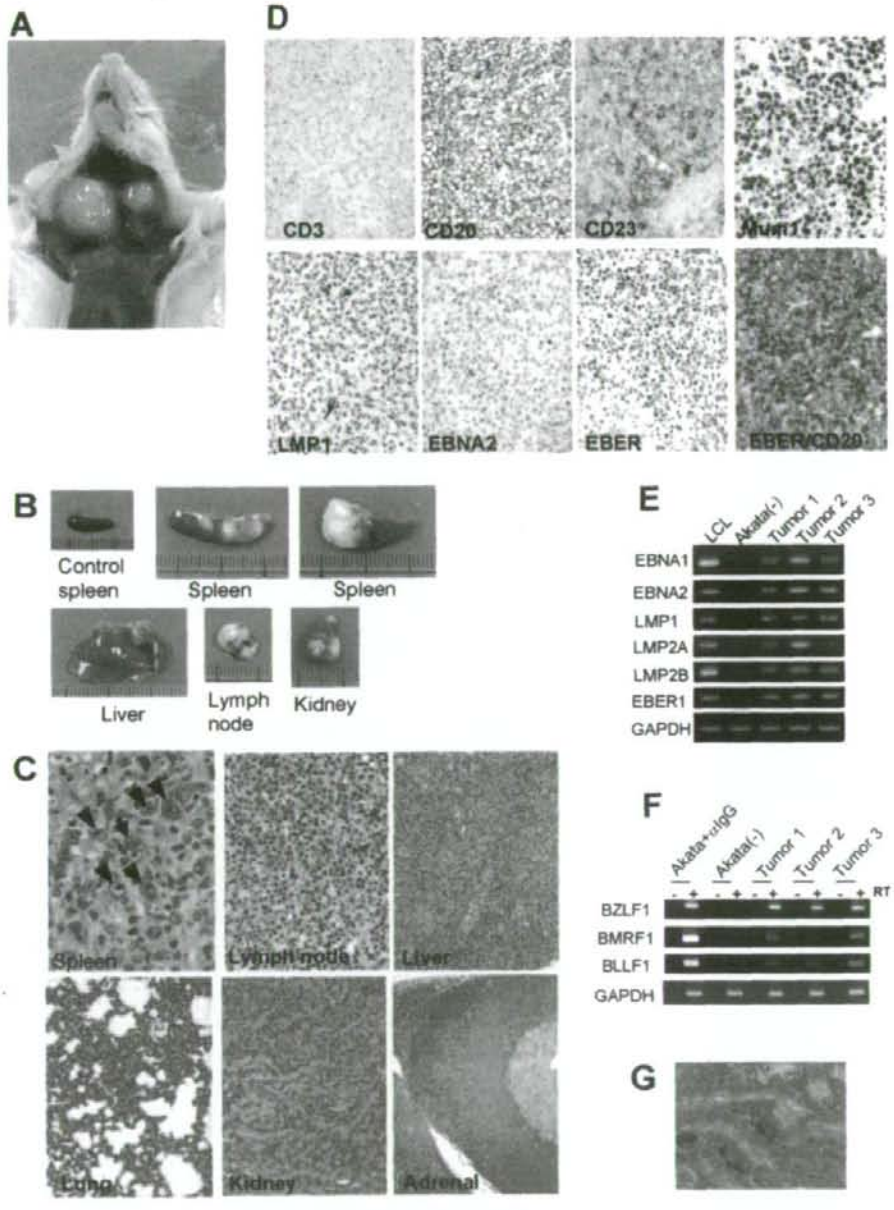

Figure 2. Pathological and virological analyses of Epstein-Barr virus (EBV)–infected humanized NOG (hNOG) mice. *A,* Photograph of an EBV-infected mouse showing tumors in the cervical area. *B,* Photographs of spleens, liver, lymph node, and kidney from EBV-infected mice with lymphoproliferative disorder. The upper left panel shows the spleen from an uninfected mouse. *C,* Photomicrographs of hematoxylin-eosin–stained tissues from mice with lymphoproliferative disorder. The arrow indicates a Reed-Sternberg–like cell, and the arrowheads indicate Hodgkin-like cells. Original magnifications, ×1000 for spleen, ×400 for lymph node, and ×200 for liver, lung, kidney, and adrenal gland. *D,* Immunohistochemical staining for lymphocyte surface markers (CD3, CD20, CD23, and Mum1) and EBV-encoded proteins (latent membrane protein [LMP] 1 and Epstein-Barr nuclear antigen [EBNA] 2), as well as in situ hybridization for EBV-encoded small RNA (EBER), in a lymph node from a mouse with lymphoproliferative disorder. The bottom right panel represents double staining for EBER and CD20. Original magnifications, ×200 for all except EBER/CD20, which is ×400. *E* and *F,* Reverse-transcription polymerase chain reaction detection of latent-cycle *(E)* and lytic-cycle *(F)* EBV gene expression in tumors from EBV-infected hNOG mice. Spleen tumors from 3 different mice were examined for the expression of EBNA1, EBNA2, LMP1, LMP2A, LMP2B, EBER1, BZLF1, BMRF1, and BLLF1. RNA samples from a lymphoblastoid cell line (LCL) *(E)* and anti-IgG–treated Akata cells *(F)* were used as positive controls, and an RNA sample from EBV-negative Akata cells (*E* and *F*) was used as a negative control. Assays were done with (+) or without (−) reverse transcriptase (RT) in panel F. Expression of GAPDH was examined as a reference. *G,* Double staining of EBER and CD20 in the liver of an hNOG mouse that was persistently infected with EBV without developing lymphoproliferative disorder. EBER is stained navy in the nucleus, and CD20 is stained brown in the membrane. Original magnification, ×1000.

Table 2. Quantification of Epstein-Barr virus (EBV) DNA in persistently infected humanized NOG mice.

Organ	Mouse	
	N35-1[a]	N35-3[b]
Bone marrow	ND	4.1×10^4
Spleen	6.2×10^2	5.7×10^3
Liver	ND	2.7×10^4
Lymph node (neck)	1.6×10^3	6.9×10^3
Lymph node (axilla)	ND	2.6×10^2
Lymph node (mesentery)	ND	4.1×10^2
Lungs	2.7×10^3	1.0×10^4
Kidneys	1.2×10^3	4.8×10^4
Adrenal gland	4.4×10^1	8.0×10^3

NOTE. Data are the amounts of EBV DNA measured 22 weeks after infection, in copies per microgram of DNA. ND, not detectable.

[a] Infected at 1×10^{-1} TD_{50}.
[b] Infected at 1×10^1 TD_{50}.

Detection of antibodies specific to EBV. IgM antibody to the EBV BFRF3 protein was detected by immunoblotting essentially as described elsewhere [24], except that horseradish peroxidase–conjugated antibody specific to human IgM (Beckman Coulter) was used as secondary antibody. To prepare the glutathione *s*-transferase (GST)–BFRF3 fusion protein, a DNA fragment spanning the entire coding region of BFRF3 was amplified by PCR (sense primer, 5'-GGCTCGAATTCATGGCACGCCG-GCTGCCC-3'; antisense primer, 5'-GGCTCGGATCCATAC-ACCATGTTTCGTGCCC-3') and inserted to the GST fusion vector pSGENT2, to yield the plasmid pSGENT2-BFRF3. *Escherichia coli* cells harboring pSGENT2-BFRF3 were stimulated with isopropyl β-D-1-thiogalactopyranoside to induce the expression of GST-BFRF3, which was subsequently purified by use of the Bulk GST Purification Module (GE Healthcare).

RESULTS

EBV infection in hNOG mice. Transplantation of human $CD34^+$ HSCs in NOG mice and reconstitution of the human hematoimmune system were done as described elsewhere [18, 20]. In the initial attempts at infection, 1×10^3 TD_{50} of the Akata strain of EBV was inoculated into 6 hNOG mice, and EBV DNA was demonstrated in the peripheral blood of all of them (figure 1*A*). EBV DNA was first evident at 3–4 weeks after inoculation and reached peak levels of ~1×10^6 EBV DNA copies/μg of DNA. All 6 mice became seriously ill between 5 and 10 weeks after inoculation, with signs of weight loss (figure 1*A*), general inactivity, and piloerection. In contrast, EBV DNA was not detected in the peripheral blood, bone marrow, thymus, spleen, lymph nodes, liver, kidneys, and lungs of 3 control NOG mice that were not transplanted with HSCs but were inoculated with the virus (data not shown). Similarly, no signs of EBV infection were observed in 3 control hNOG mice that were not inoculated with the virus (data not shown). In total, 43 NOG mice that had been humanized with HSCs from 9 different cord blood samples were inoculated with 1×10^3 TD_{50} of EBV, and in 38 of them the results were similar to those observed in the initial 6 mice, with high blood EBV load and severe deterioration in their general condition. Ten of them died and could not be examined further. The remaining 28 mice were killed, and signs of lymphoproliferative disorder were found at autopsy (see the below). These results demonstrate that hNOG mice can be infected with EBV, with a mostly fatal outcome at this virus dose.

EBV-induced lymphoproliferative disorder in hNOG mice. Autopsy of killed mice showed signs of lymphoproliferative disorder typically represented by an overt tumor in the spleen (figure 2*B*). In ~70% (20/28) of the mice autopsied, macroscopical signs of disseminated disease were found in the liver, lymph nodes, or kidneys (figure 2*A* and 2*B*). Seventeen mice were examined pathologically, and 15 of them showed typical histology of diffuse large B cell lymphoma, with remarkable similarity to the human lymphoproliferative disorder in the immunocompromised hosts (figure 2*C*). The tissues contained occasional immunoblasts, Reed-Sternberg–like cells, and Hodgkin-like cells (figure 2*C*). Marked infiltration of large transformed lymphoid cells was also demonstrated in liver, lymph nodes, kidneys, adrenal glands, and lungs (figure 2*C*). Real-time PCR detected high levels (~1×10^5 to ~1×10^6 EBV DNA copies/μg of DNA) of EBV DNA in these organs, and the large transformed lymphoid cells were universally EBV positive by EBER ISH (figure 2*D*). Immunohistochemical analysis showed that the large transformed lymphoid cells were of the activated B cell phenotype, being reactive for CD20 and CD23 and not reactive for CD3 and CD10 (figure 2*D* and data not shown). They were also positive for Mum-1, a late- and postgerminal center cell marker. The EBER-positive cells were CD20-positive B cells (figure 2*D*), and no EBER-positive T cells were identified. Immunostaining revealed that most proliferating cells expressed EBNA2, whereas LMP1 was expressed in only a fraction of them (figure 2*D*). RT-PCR analysis of typical spleen tumors obtained from 3 different mice showed the expression of EBNA1, EBNA2, LMP1, LMP2A, LMP2B; and EBER, consistent with the latency III program of EBV gene expression (figure 2*E*). In addition, transcripts from lytic-cycle EBV genes, including BZLF1 (immediate-early), BMRF1 (early), and BLLF1 (late, encoding gp350/220), were identified (figure 2*F*).

Virus dose–dependent outcome of EBV infection in hNOG mice. To examine the influence of virus dose on the outcome of EBV infection, we inoculated serial dilutions of EBV preparation into 2 lots of hNOG mice, each consisting of 5 mice that had been humanized with the same HSC preparation. Consistent with the results described above, the 4 mice (2 from each lot) that received the higher doses (1×10^3 and 1×10^2 TD_{50}) of the

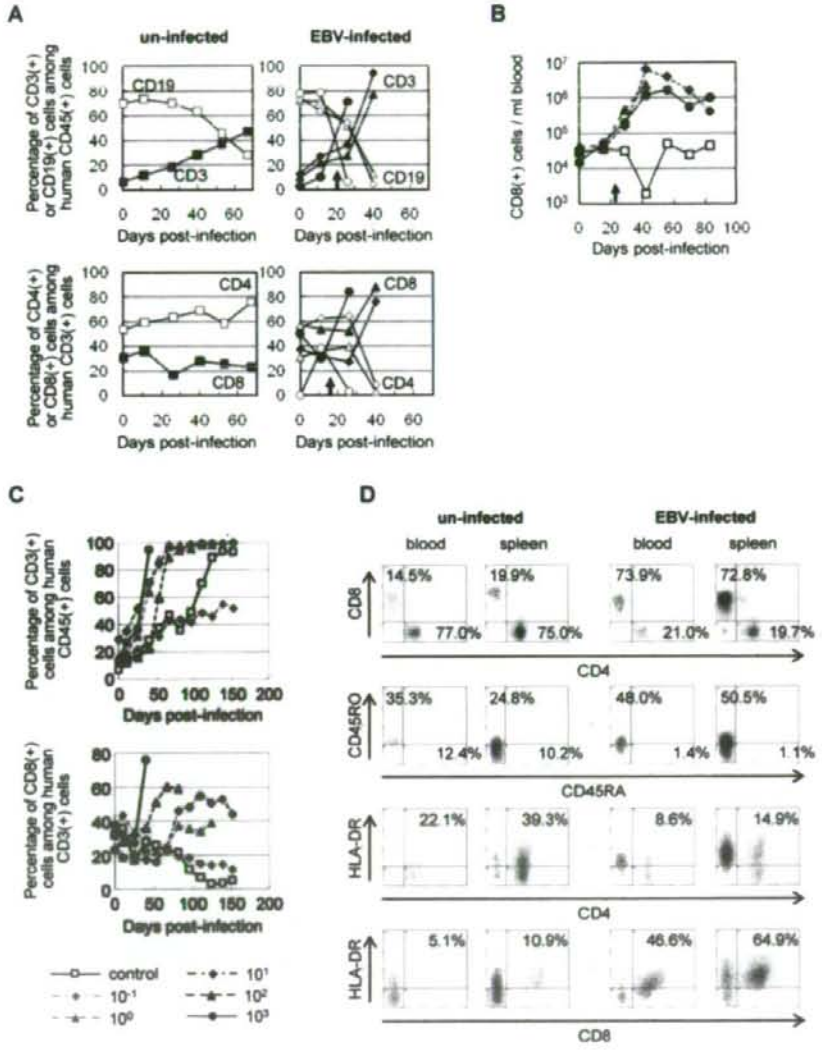

Figure 3. Surface marker expression by peripheral blood T cells in Epstein-Barr virus (EBV)–infected humanized NOG (hNOG) mice. *A,* Changes in the percentages of $CD3^+$ T cells and $CD19^+$ B cells among human $CD45^+$ leukocytes *(upper panels)* and in the percentages of $CD8^+$ cells and $CD4^+$ cells among $CD3^+$ cells *(lower panels)* after infection with EBV. Results obtained from 3 EBV-infected mice and an uninfected mice are shown. White symbols indicate the percentage of $CD19^+$ cells *(upper panels)* or $CD4^+$ cells *(lower panels);* black symbols indicate the percentage of $CD3^+$ cells *(upper panels)* or $CD8^+$ cells *(lower panels).* A vertical arrow in the graph area shows the time point at which EBV DNA was first detected in peripheral blood. *B,* Changes in the no. of $CD8^+$ T cells in the peripheral blood of EBV-infected hNOG mice. White symbols indicate uninfected mice, and black symbols indicate infected mice. Note that cell no. is plotted in a logarithmic scale. *C,* Viral dose–dependent T cell responses in hNOG mice inoculated with serially diluted EBV. Ten-fold serial dilutions of an EBV sample starting from 1×10^3 TD_{50} per inoculate were injected intravenously into NOG mice that had undergone transplantation with the same lot of human hematopoietic stem cells (HSCs). Changes in the percentages of $CD3^+$ T cells among human $CD45^+$ leukocytes *(upper panel)* and in the percentages of $CD8^+$ cells among $CD3^+$ cells *(lower panel)* after inoculation with EBV are shown. The viral dose for each mouse is shown in the key. *D,* Comparison of surface marker expression between EBV-infected mice and control mice. Two mice that underwent transplantation with the same lot of human HSCs were either inoculated with EBV or left uninfected; 10 weeks after inoculation, mononuclear cells obtained from peripheral blood or spleen were gated for the expression of human CD3 and then examined for the expression of CD8 and CD4 *(top panels),* CD45RO and CD45RA *(second from top),* HLA-DR and CD4 *(second from bottom),* and HLA-DR and CD8 *(bottom).*

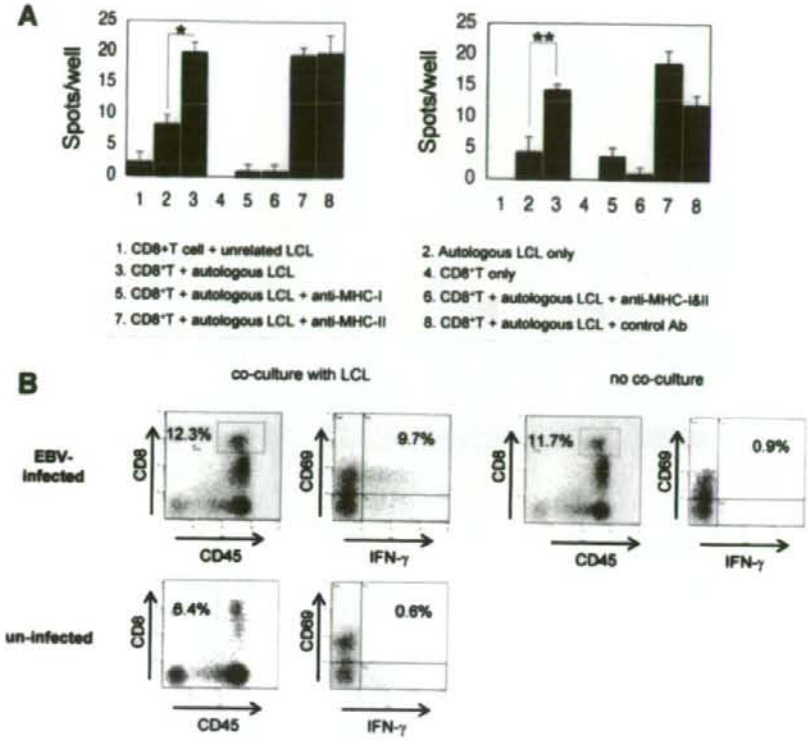

Figure 4. Epstein-Barr virus (EBV)–specific T cell response in humanized NOG (hNOG) mice. *A*, Enzyme-linked immunospot assay for the detection of human T cells producing interferon (IFN)–γ after stimulation with an EBV-positive lymphoblastoid cell line (LCL). $CD8^+$ cells isolated from EBV-infected hNOG mice were cocultured with an autologous LCL, and IFN-γ–secreting cells were counted (3, 5, 6, 7, and 8). To analyze restriction by major histocompatibility complex (MHC), antibody to HLA class I (anti–human HLA-ABC clone W6/32; eBioscience) (5), antibodies to both HLA class I and class II (6), antibody to HLA class II (anti–human HLA-DP,DQ,DR clone CR3/43; Dako) (7), or isotype-matched control antibody (8) were added to the culture. Control experiments included coculture of $CD8^+$ cells with an MHC-mismatched LCL (1), culture of the autologous LCL only (2), and culture of $CD8^+$ cells only (4). Results from 2 infected mice are shown. Five hundred $CD8^+$ cells per well were cultured in the experiment shown on the left, and 250 $CD8^+$ cells per well were cultured in that shown on the right. Spots were counted in triplicate in each of the 8 experimental groups, and the bars represent mean values and SEs. The unpaired Student's *t* test was used for statistical analysis. $^*P < .01$ and $^{**}P < .02$. *B*, Detection of human $CD8^+$ cells that produce IFN-γ in response to stimulation with an EBV-positive LCL by flow cytometry. $CD8^+$ cells were isolated from the spleen of an EBV-infected mouse and cocultured with the autologous LCL. Intracellular IFN-γ was stained and analyzed as described in Methods.

virus died of lymphoproliferative disorder ~5–10 weeks after inoculation. The remaining mice in both of the lots that received lower doses (1×10^1, 1×10^0, and 1×10^{-1} TD_{50}) survived acute infection and appeared normal throughout the observation period of 22 weeks. Although EBV DNA was detected at variable levels in their peripheral blood several weeks after inoculation, it returned to undetectable levels thereafter (figure 1*B*), suggesting that a certain protection mechanism worked to control EBV infection. Importantly, EBV DNA could be still detected in various organs, including spleen, liver, lungs, kidneys, and adrenal glands, at the end of the observation period (22 weeks), indicating that EBV persisted in these mice (table 2). Double staining for EBER and CD20 showed that EBV persisted in B cells (figure 2*G*). Macroscopical examination by autopsy at the end of the observation period did not reveal abnormality in these mice, except for moderate splenomegaly found in a mouse that received 1×10^1 TD_{50}. These results indicate that the outcome of EBV infection in hNOG mice varies with the virus dose; high doses of virus tend to cause fatal lymphoproliferative disorder, whereas lower doses induce apparently asymptomatic persistent infection.

EBV-specific T cell response in hNOG mice. Flow cytometry analysis demonstrated a dramatic increase in the percentage of $CD3^+$ T cells among the human $CD45^+$ leukocytes after infection with EBV. This increase in T cells was accompanied by an increase in the percentage of $CD8^+$ cells among human $CD3^+$ T cells. These changes were seen in virtually all infected mice, and the results from 3 mice are shown in figure 3*A*. The slow increase in the percentage of $CD3^+$ cells in the uninfected mouse represents the process of humanization (i.e., the development of hu-